AD

STUDY OF 2D AND 3D BOUNDARY LAYER OF MOVING WALLS BY EMBEDDED LDV MEASUREMENTS

Final Technical Report
by
Christian. Maresca, Eric. Berton, Daniel. Favier and Amine Benyahia

Laboratoire d'Aérodynamique et de Biomécanique du Mouvement
163 Av. de Luminy, Case 918
13288 marseille cedex 09. France

(Mach 2002)

United States Army

EUROPEAN RESEARCH OFFICE OF THE U.S. ARMY

London, England

CONTRACT NUMBER N 68171-01-M-5090

Contractor: M. Laurent, Président de l'Université de la Méditerranée

REPORT DOCUMENTATION PAGE

Form Approved OMB No. 0704-0188

1. REPORT DATE (DD-MM-YYYY)	2. REPORT TYPE	3. DATES COVERED (FROM - TO)
10-03-2002	Final rept.	02-11-2000 to xx-11-2001

4. TITLE AND SUBTITLE
Study of 2D and 3D Boundary Layer of Moving Walls by Embedded LDV Measurements
Unclassified

5a. CONTRACT NUMBER
N68171-01-M-5090

5b. GRANT NUMBER

5c. PROGRAM ELEMENT NUMBER

6. AUTHOR(S)
Maresca, Christian ;
Berton, Eric ;
Favier, Daniel ;
Benyahia, Amine ;

5d. PROJECT NUMBER

5e. TASK NUMBER

5f. WORK UNIT NUMBER

7. PERFORMING ORGANIZATION NAME AND ADDRESS
LABM, CNRS-University of la M#terran#
163 Av. de Luminy, Case 918
13288 Marseille, Cedex 009, Francexx

8. PERFORMING ORGANIZATION REPORT NUMBER

9. SPONSORING/MONITORING AGENCY NAME AND ADDRESS
United States Army
European Research Office of the U.S. Army
London, England

10. SPONSOR/MONITOR'S ACRONYM(S)

11. SPONSOR/MONITOR'S REPORT NUMBER(S)

12. DISTRIBUTION/AVAILABILITY STATEMENT
APUBLIC RELEASE
,

13. SUPPLEMENTARY NOTES
See also ADM001379, non print version.

14. ABSTRACT
See report.

15. SUBJECT TERMS

16. SECURITY CLASSIFICATION OF:			17. LIMITATION OF ABSTRACT	18. NUMBER OF PAGES	19. NAME OF RESPONSIBLE PERSON
a. REPORT	b. ABSTRACT	c. THIS PAGE	Public Release	40	ADM001379, see non-print manager for disk, (blank) lfenster@dtic.mil
Unclassified	Unclassified	Unclassified			19b. TELEPHONE NUMBER International Area Code Area Code Telephone Number 703767-9007 DSN 427-9007

REPORT DOCUMENTATION PAGE			
1.Agency Use Only	2.Report Date : 10 MARCH 2002	3.Type of Report and Dates Covered : Final Report 2 NOV 2000-NOV2001	
4.Titles and Subtitle: Study of 2D and 3D boundary layer of moving walls by embedded LDV measurements			5.Funding Numbers : C N 68171-01-M-5090
6.Author(s): C. Maresca, E. Berton, D. Favier and A. Benyahia			
7.Performing Organization Name(s) and Adresse(s) : LABM, CNRS-University of la Méditerranée. 163 Av. de Luminy, Case 918 13288 Marseille, Cedex 009, France			8. Performing Organization Report Number : 04-IR
9.Sponsoring/Monitoring Agency Name(s) and Adresse(s)			10. Sponsoring/Monitoring Agency Report
11.Supplementary notes			
12a.Distribution/Availability Statement :public availability			12b.Distribution Code

13.Abstracts : The present final report concerns the extension of the seed contract to more new 2D and 3D tests in order to provide the Aeromechanics of the Army/NASA Rotorcraft Division with experimental results on BL velocity profiles and on the structure of unsteady separated 2D and 3D flows

Smoke visualization and embedded laser velocimeter (2D and 3D) operating in the backscatter mode were used to survey the separation bubble and the flow about 2D and 3D wings oscillating in the wind tunnel S2Luminy.

The experiments were carried out about two rectangular wings with a NACA 0012 airfoil section oscillating in pitch, one spanning the entire test section (2D configuration), the other only the half section (3D configuration). During the oscillation, the wing angle of attack varied around mean values α_0=6deg and 12deg through an angle amplitude $\Delta\alpha$=± 6deg, at reduced frequency k=0.188, and at nominal Reynolds numbers $R_e=10^5$. The measurements of 2 and 3 orthogonal components of instantaneous velocity through the boundary layer along a normal to the surface of the wing have shown that the embedded 2D and 3D laser velocimeters are well suited to characterize qualitatively and quantitatively the structure of the boundary layer (laminar, transition, turbulent, turbulence intensity and Reynolds stresses), as well as strong separation with leading edge bubble involved during dynamic stall. Geometry and behavior of the separation bubble on the upper side of the airfoils were investigated from velocity profiles. These results constitute a useful database for future computational unsteady boundary layer.

14.Subject terms: Dynamic stall. Boundary layer. Visualization. Laser light sheet. Image processing.	15.Number of Pages 40
	16.Price Code

17.Security Classification Unclassified	18. Security Classification of this Page Unclassified	19.Security Classification of Abstract Unclassified	20.Limitation of Abstract UL

SUMMARY

Basic knowledge and numerical investigation of rotary wings aerodynamics request more and more accurate and suited experimental data. Particularly, phenomena occurring in the region very close to the blades, like transition, separation, and dynamic stall are highly dependent on the local boundary layer (BL). Flow visualization and instantaneous velocity profiles remain useful and suitable tools for analyzing the behavior of BL and for collecting information.

LABM (Laboratoire d'Aérodynamique et de Biomécanique du Mouvement) from CNRS and University of la Méditérranée (Marseille) has already performed[1], through a seed ERO contract (Nb N68171.99.M6670), visualizations and embedded LDV velocity measurements of the BL developed on a 2D pitching airfoil.

The present final report concerns the extension of the seed contract to new 2D and 3D tests in order to provide the Aeromechanics of the Army/NASA Rotorcraft Division with experimental results on BL velocity profiles and on the structure of unsteady separated 2D and 3D flows.

Smoke visualization and embedded laser velocimeter (2D and 3D) operating in the backscatter mode were used to survey the separation bubble and the flow around 2D and 3D wings oscillating in the S2Luminy wind tunnel.

The experiments were carried out on two rectangular wings with a NACA 0012 airfoil section oscillating in pitch, one spanning the entire test section (2D configuration), the other spanning only the half section (3D configuration). During the oscillation, the wing angle of attack varied around mean values α_0=6deg and 12deg through an angle amplitude $\Delta\alpha$=± 6deg, at reduced frequency k=0.188, and at nominal Reynolds numbers $R_e=10^5$. The previous work[1] has shown that the basic flow features are independent of Reynolds Number at least in the range 10^5-10^6.

The measurements of 2 and 3 orthogonal components of instantaneous velocity through the boundary layer along a normal to the wing surface have shown that the embedded 2D and 3D laser velocimeters are well suited to characterize qualitatively and quantitatively the structure of the boundary layer (laminar, transition, turbulent, turbulence intensity and Reynolds stresses), as well as strong separation with leading edge bubble involved during dynamic stall. Geometry and behavior of the laminar separation bubble on the upper side of the airfoils were moreover investigated from measured velocity profiles. These results constitute a useful database for future computational unsteady boundary layer and CFD methods.

List of Keywords: Dynamic stall, Boundary layer, Bubble separation, Laser light sheet visualization, Embedded Laser Doppler Velocimeter, Image processing.

INTRODUCTION

Dynamic stall occurring on the retreating blade of a helicopter rotor in forward flight has been widely investigated using oscillating 2D models in wind-tunnels. The physical flow features of the stalling process, have been delineated on airfoils oscillating either in pitch[2-4] or in fore and aft-pitching combined motion[5-7]. More recently, W. G. Bouseman[8] has shown that the loading, characterized by the peak airfoil lift and drag, and the minimum pitching moment, termed the "dynamic stall function", is similar over a wide range of test conditions including flight tests. In particular, the dynamic stall function appears to be relatively insensitive to Reynolds number and shows that an accurate prediction of 3-D effects is not of prime importance for the prediction of dynamic stall on a flight vehicle.

These results encourage to enforce numerical methods presently developed for the direct calculation of dynamic stall by solving the Navier-Stokes equation[9] but limited to 2D flow at low Reynolds number. These challenging methods are at a research stage and their validation and improvement require more accurate and suited experimental data to bring some help to theoreticians and numericians for understanding the separation process and for being capable of accounting for transition of B.L. Moreover, tip vortex effect of oscillating models in wind tunnel on dynamic stall has to be evaluated and compared to conclusions given by Bouseman on flight test dynamic stall from flight tests.

So, the purpose of the present work was to extend experiments based on flow visualization and velocity measurements in the boundary layer to unsteady transition and separation in 2D and 3D flows. The laser sheet visualization and the embedded LDV techniques developed at LABM[10] have been extended to 3D within the frame of the contract and are shown to be well suited to characterize the flow physics features generated by transition (laminar bubble) and dynamic stall phenomena occurring on oscillating airfoils.

In the first phase, the work has been undertaken on an airfoil oscillating in 2D attached flow configuration to characterize the unsteady transition from laminar to turbulent (behavior of the bubble under

oscillating conditions). A particular attention has then be paid to the unsteady separation occurrence when the airfoil is oscillating through dynamic stall. The structure of the flow field at the inception of separation, and at the growing and bursting of the laminar bubble as incidence was increasing and decreasing has been studied qualitatively and quantitatively by use of our unique embedded LDV and flow visualization techniques.

In the second phase, a half wing of the same airfoil has been experienced in the same wind tunnel in order to evaluate the effects of span and of tip vortex (3D effects) on transition and separation. Visualizations and velocity profiles in the boundary layer at different locations in chord and span (3D case) have been performed.

The study has been realized in S2Luminy wind-tunnel at a Reynolds number of 10^5 (Mach Number 0.015).

The 2D and 3D models, of NACA0012 airfoils, were oscillating in pitch around 2 mean angles of attack α_0, at a reduced frequency k and an amplitude of incidence $\Delta\alpha$ relevant to the retreating helicopter rotor blade (k=0.188, α_0=6deg and 12 deg, $\Delta\alpha$=6deg).

The formation and shedding of vortices generated by the dynamic stall have been observed using a laser sheet visualization technique. Movies showing separation and reattachment during dynamic stall have been compared in 2D and 3D configurations.

The velocity components (U= U(ωt), V=V(ωt), W=W(ωt)) have been measured in the BL from y=0.1mm at the wall to 100 mm outside of the BL. Inside the BL, measurements have been performed at every altitude step of 0.2 mm. Turbulence intensity and Reynolds stresses have been deduced from the instantaneous velocity values.

SYMBOLS

C	Airfoil chord, m
f	Frequency, Hz
h	Airfoil span, m
k	Reduced frequency, $k=C\omega/2U_\infty$
Re	Reynolds number, $Re=U_\infty C/\nu$
U_∞	Wind tunnel velocity, m/sec
U,V, W	Tangential normal and longitudinal velocity, m/sec
s	Curvilinear abscissa, m
t	Time, sec
x, y,z	Tangential normal and spanwise coordinate at the airfoil surface, m
α	Angle of attack of the airfoil, deg
α_0	Mean angle of attack, deg
$\Delta\alpha$	Amplitude of the pitching oscillation, deg
δ	Thickness boundary layer, m
η	Reduced normal coordinate, $\eta=y(Re_x)^{1/2}/x$
ω	Rotational frequency, rad/sec

EXPERIMENTAL INVESTIGATION

The wind tunnel

S2Luminy low speed (Fig.1) is an open circuit wind-tunnel with rectangular closed section (1mx0.5m) 3m in length, free stream velocity varying from 2.5m/s to 25m/s, natural turbulence intensity less than 0.5%.

Oscillating airfoils

Airfoils used are of NACA0012 profile. One of them (2D) is 0.30m in chord, 0.4951 m in height, with one tip mounted flush to the floor of the test section, the other (3D) is 0.3m in chord and 0.25m in height. The pitching motion of the airfoil is allowed by means of an oscillating device located under the test section (see Fig.1) and supporting vertically the model by means of a support shaft located at the quarter chord axis. In this way, the instantaneous incidence $\alpha(t)$ of the airfoil is given by:

$$\alpha(t)= \alpha_0+\Delta\alpha\sin(\omega t),$$

where α_0 is the mean incidence and ω the rotational frequency.

The following table summarizes the experimental conditions realized:

Table 1

	U_∞: m/s	C: m	h: m	Re	f=2π/ω: Hz	k	α_0: deg	Δα: deg
S2L,2D	5	0.3	0.495	10^5	1	0.188	6; 12	6
S2L,3D	5	0.3	0.25	10^5	1	0.188	6; 12	6

Visualization

The technique consists in illuminating the mid-span of the airfoil while the flow is seeded upstream with oil smoke emitted through a tube rake. The light sheet is produced from an optical system mounted flush with the wall of the wind tunnel in order to avoid light reflection. The optical system, manufactured by Dantec, is composed of a glass cylinder and a converging lens connected by an optical fiber to a laser source (Spectra-Physics 12 Watts). Figure 2 sketches the set-up realized in S2L. It can be seen that the light sheet has been adjusted to illuminate the middle horizontal plane of the wind tunnel. During tests, pictures of the flowfield close to the airfoil are taken from a digital camera (Olympus Camedia C-2500L) synchronized on the motion of the oscillating airfoil. These pictures are processed through "Adobe Photoshop" software in order to capture the features of the flowfield. Moreover, movies have been realized from the pictures shot at different instant of the period of oscillation. This technique has been described in details in the previous report[1].

Velocity measurements

For each chordwise section selected, the flow survey is performed along the local normal to the wall surface (the altitude Y ranging from about 0.1 mm to 100mm).

2D velocimetry.

The Embedded Laser Doppler Velocimeter[7] (ELDV) used for this survey in 2D flow has an optical head mounted on a supporting turntable linked to the oscillating frame as sketched in Fig.3. Moreover, it is equipped with a beam-expander to increase the focal distance to 400mm. This optical head is installed on an automated 2D-displacement device mounted itself on the turntable. The laser beams are so focusing from a 45deg mirror in the boundary layer at the spanwise locations considered. The supporting turntable is linked with the oscillating frame, so that U and V velocity components can be directly measured in the same reference frame as the oscillating BL. A teledriven system allows the adequate positionning of the measurement volume at any point of the airfoil surface (30cm in chordwise displacement). An angular sector provides the selection of the surveying normal direction, and the laser measurement volume can be displaced along the local normal to the surface with a displacement accuracy of 0.1mm. Due to the periodicity of the flow, each period is considered as a specific sample of the same phenomenon. So, each velocity component is recorded at each phase angle ωt ranging from 0deg to 360deg by step of 1deg over a large number of periods. Data are then statistically analyzed at prescribed values of the period, e.g. the instantaneous incidence, with an accuracy of $\delta\alpha=4\Delta\alpha/360=24/360=0.066$deg. The acquisition time is stopped when 19,564 data have been stored, that generally requires about 150 periods.

Data acquisitions are made on a microcomputer from two Burst Spectrum Analyser delivering the values of the two components U and V and the arrival validation time for each frequency measurement. The software used for acquisition and data reduction (COMBSA) has been developed at LABM under Apple LabVIEW system.

3D velocimetry.

The extension of the Embedded Laser Doppler Velocimetry (ELDV) method to the direct measurement of the 3D velocity field has been performed by means of special arrangements of mirrors and laser optical heads sketched at the top of Fig.4. The system consists in two optical heads mounted on a supporting turntable and attached to the oscillating frame (presented at the bottom of Fig.4). Mirror 1 collects purple beams from the 1D optical head and mirror 2 green and blue beams from the 2D optical head.

Green beams issued from mirror 2 and purple beams issued from mirror 1 are in a vertical plane and converge in a measurement volume giving the components Ug and Up (see top of figure 5).

Blue beams from mirror 2 give directly the Ub component (bottom of Fig.5). The 3D velocity components are then given by:

$$\mathbf{U} = \frac{\sqrt{2}}{2}(\mathbf{Ug} + \mathbf{Up}),\ \mathbf{V} = \mathbf{Ub},\ \text{and}\ \mathbf{W} = \frac{\sqrt{2}}{2}(\mathbf{Ug} - \mathbf{Up})$$

A particular attention has been paid to the process used for the turbulence determination from the velocity signal. Thus, the new procedure of data acquisition involves only a given phase that can be repeated along the oscillation cycle. This acquisition procedure "phase by phase" makes sure that the three components of the velocity are measured by the ELDV method, along the same cycle and at the same time.

This condition secures the validity of the velocity fluctuation measurements required for the Reynolds stress consideration.

RESULTS AND DISCUSSION

Velocity components and turbulence results in the boundary layer

All boundary layer data acquired using the 2D and 3D embedded LDA are summarized in table 2 and have been stored on CD Rom

2D steady airfoil : $Re=10^5$ ($U_\infty=5ms^{-1}$)

Test conditions			Boundary layer data		
$\bar{z}$	x/c	$\alpha_0$deg	U,V	$\sigma u,\sigma v$	$\overline{u'v'}$
0.5	0.25	6, 12	x	x	x

3D steady airfoil : $Re=10^5$ ($U_\infty=5ms^{-1}$)

Test conditions			Boundary layer data		
$\bar{z}$	x/c	$\alpha_0$deg	U,V,W	$\sigma u,\sigma v,\sigma w$	$\overline{u'v'}$
0.6, 0.8	0.13, 0.25, 0.40	0, 6, 12, 18	x	x	x

2D oscillating airfoil : $Re=10^5$ ($U_\infty=5ms^{-1}$), k=0.188

Test conditions				Boundary layer data at Ψ=0, 45, 90, 135, 180, 225, 270, 315deg		
$\bar{z}$	x/c	$\alpha_0$deg	Δα deg	U,V	$\sigma u,\sigma v$	$\overline{u'v'}$
0.5	0.25	6, 12	6	x	x	x

3D oscillating airfoil : $Re=10^5$ ($U_\infty=5ms^{-1}$), k=0.188

Test conditions				Boundary layer data at Ψ=0, 45, 90, 135, 180, 225, 270, 315deg		
$\bar{z}$	x/c	$\alpha_0$deg	Δα deg	U,V,W	$\sigma u,\sigma v,\sigma w$	$\overline{u'v'}$
0.6, 0.8	0.13, 0.25, 0.40	6, 12	6	x	x	x

Table 2 : Boundary layer data

The results analysis has consisted in comparing velocity and turbulent components obtained on the 3D airfoil for a fixed x/c=0.25, at z/h=0.8 and 0.6, with the 2D results obtained at z/h=0.5. Figures 6 to 17 describe the components measured normally to the airfoil surface from Y=0.1mm to Y=70mm. Some typical results of the steady and oscillating boundary layer have been underlined by zooming the closer surface location between Y=0.1mm and Y=6mm in figures 18 to 23.

Results obtained at other chord stations (x/c=0.13, and x/c=0.4) have also been analyzed and have allowed the study of the behavior of the laminar bubble of transition during the oscillation of the airfoil in the 3D configuration.

Results analysis at x/c= 0.25

Steady boundary layer results are presented in figures 6 to 9. The 3 components U, V, W, the turbulence intensities $\sigma u,\sigma v,\sigma w$ in m/s and the Reynolds stress $\overline{u'v'}$ in m^2/s^2 are shown for α=0, 6, 12, and 18deg and for z/h=0.6 and 0.8 in the 3D configuration. Moreover, it has been possible to compare 3D with 2D results at α=6, and 12deg in Figures 7 and 8. Concerning low incidence results ($\alpha \leq 12$deg, Fig.6 to Fig.8), it can be seen that the main effect of the wing tip is a decrease of the U component intensity in the boundary layer and in the potential flow surrounding the airfoil when z/h is increasing from 0.6 to 0.8. This is due to the reduction of the effective incidence of the airfoil induced by the tip vortex, more intensively close to the tip (z/h=0.8) than inboard (z/h=0.6). This is confirmed by the 2D results of Fig.7 and Fig.8 unaffected by tip vortex. It can also be observed that the U difference between tip and inboard spanwise locations increases with the incidence as the tip vortex grows also with incidence. At 0deg the V component remains very close to 0 m/s with a tendency to become positive in the boundary layer when approaching the tip region. Higher incidences (6, 12deg), indicate a weak effect on the V component and when compared to steady values of

Fig.7 and Fig.8, it becomes difficult to point out the tip vortex effect. When looking at the W components, it can be noticed that the effect of tip vortex results is an increase of downwash velocity at the tip. The level of turbulence measured on the three components is more difficult to analyze. Nevertheless, it appears that the tip vortex weakens the turbulence level in the boundary layer at z/c=0.8, and inversely increases the Reynolds stress. At higher incidence (α=18deg, Fig.9), the U components show that the reverse flow is stronger inboard at z/h=0.6 than close to the tip at z/h=0.8, indicating the reattachment effect of the vortex at the tip of the airfoil.

Unsteady boundary layer results on the oscillating profile are presented in figures 10 to 13 for incidence oscillating through conditions: α_0=6deg, $\Delta\alpha$=6deg, and in figures 14 to 17 for: α_0=12deg, $\Delta\alpha$=6deg. The velocity components U, V, W, are presented in Fig10 at instantaneous incidence : α=0deg and α_0=12deg corresponding to lowest and highest instantaneous incidences during the oscillation. Values obtained at z/h=0.6 and z/h=0.8 are compared to steady values presented in Fig.7 and Fig.8. In a same way, Fig.11 gives the intensity components and the Reynolds stress, as Figures 12 and 13 are relative to instantaneous incidence 6deg: the first one when reached by increasing incidence, the second by decreasing incidence.

The global analysis made on these results concerning low incidences lead to the conclusion already made on steady results that the main effect of the tip effect is a reduction of the instantaneous incidence induced by the tip vortex. In the present experimental conditions we can speak about a quasi-steady behavior of the boundary layer with respect to the intensity of the tip vortex during the period. Looking now at results related to higher incidences and dynamic stall (Figures 14 to 17), it is worthy of note that a reattachment of the boundary layer close to the tip at z/h=0.8 can be observed at the incidence : α=18deg, and that the boundary layer remains separated at z/h=0.6. The effect of flow reattachment produced by the tip vortex, previously shown in steady flow conditions is confirmed in the oscillating case. The other results shown in the figures for unstalled incidences (6 and 12deg) exhibit a quasi-steady BL behavior.

For a better understanding of the boundary layer behavior, the region close to the airfoil surface has been zoomed between y=0.1mm and Y=6mm for typical results previously presented in figures 6 to 17. Figures 18 and 19 present steady velocity and turbulence components in the boundary layer at 6deg and 18 deg. When the flow is attached (Fig.18), it can be noticed that the tip vortex does not highly affect the U component but induces a higher negative normal velocity V resulting in a better attachment of the flow to the surface. A downwash velocity characterized by negative values of W appears close to the tip (z/h=0.8). In separated steady flow at α=18deg (Fig.19) the benefic effect of the tip vortex on the reattachment of the boundary layer can be observed particularly on the U component.

When the airfoil oscillates in a non-dynamic stall regime ($0\leq\alpha\leq12$deg), the boundary layer behavior during upstroke and downstroke is presented in Fig20 (velocity components) and Fig21 (turbulence components). It can be deduced from such results that no new typical effect previously mentioned on the tip effect is to be emphasized.

When the airfoil undergoes dynamic stall ($6\leq\alpha\leq18$deg), boundary layer components in Fig.22 (velocity), and in Fig.23 (turbulence) corresponding to the lowest incidence (6deg) and the highest (18deg) of the oscillation clearly show the reattachment of the flow at 18deg, characterized by the positive values of the U component and by the decrease of the turbulence compared to steady case.

Results analysis at different x/c. Transition bubble analysis.

Variations with time of the U component has been analyzed along the period of oscillation for x/c=0.13, 0.25, and 0.4, at different normal position Y ranging from 0.1mm to 70mm when the incidence varies in the non-dynamic stall regime $0\leq\alpha\leq12$deg. The experimental set up produces a sinusoidal variation of the incidence decreasing from 12deg to 0deg during the first half of the period and increasing from 0deg to 12deg during the last half part of the period.

Assuming that the transition of the boundary layer results from a laminar separation bubble as shown in Fig.24, some remarks supporting the following analysis have to be made:

1- The bubble moves towards the leading edge and grows in size when the incidence increases. Reciprocally, it moves towards the trailing edge and reduces when the incidence decreases.

2- Assume now that the measurement volume giving the U component at the altitude Y is located at a point A inside the bubble at a given incidence of the period of oscillation (see Fig.24). If the incidence is decreasing, as long as Y remains inside the bubble, the component U indeed increases because the bubble reduces and the measuring volume moves closer and closer to the external flow.

3- Assume finally that the incidence has sufficiently decreased in such a way that the altitude Y has emerged out of the bubble (point B, in Fig.24), the U component will then decrease as incidence will continue to decrease.

In summary it can be concluded that as long as the measurement volume remains inside the bubble during the oscillation, the U component varies out of phase of the incidence, and in phase with the incidence when out of the bubble. If during the oscillation a change of “in phase to out of phase variation” can be observed, the height of the bubble at the chord station x/c considered is given by the value of Ymm at the corresponding incidence.

The figure 25 illustrates three typical records of the variation of Um/s with the incidence. The record at the top of the figure concerns the leading edge (x/c=0.13) and a normal position very close to the surface (Y=0.2mm). It can be observed that between 12 and 9deg (points A to B), the measurement volume is inside the bubble in the region of negative velocity, and between 9 and 3deg (points B to C), U varies out of phase of the instantaneous incidence, which means that Y remains inside the bubble. When the incidence reaches 3deg, the measurement volume goes out of the bubble, indicating a bubble height of Y=0.2mm at this incidence. The measurement volume remains outside of the bubble between points B and C and reenters the bubble at point D. The second record in the middle of the figure concerns the same chord station at a higher normal location Y=1 mm. The entering in the bubble occurs during upstroke at point D where the incidence is higher than the one corresponding to a lower position Y (top of the figure), and the exit is indicated by point C during downstroke where the incidence is also higher than the one observed at lower Y. The bottom of the figure is relative to the chord station x/c=0.25, z/h=0.8 and Y=2mm. This record, relative to a different z/h, confirms the previous observations and shows clearly that the bubble is 2mm in height at 6.7deg during downstroke (point C), and keeps the same height at 6.9deg deg during upstroke (point D). Such analysis have been made for all U records at x/c=0.13, 0.25, and 0.4, for Ymm=0.1, 0.2, 0.4, 0.6, 0.8, 1, 1.5, 2, 3, 4, 6, 8, 10, 15, 20, 40, 50,and 70, for z/h=0.6 and 0.8.

Thus, the variation with incidence of the height of the bubble can then be drawn for the 3 chord stations at 2 different span locations. Figures 26 and 27 concern bubble heights obtained respectively at z/h=0.6, and z/h=0.8. For each chord station x/c=0.13, 0.25, and 0.4 the variations of the bubble height has been plotted versus upstroke and downstroke incidences. The bubble is higher during downstroke and weakens in size when the tip of the airfoil is approached, as shown in Fig.28 where the results at z/h=0.6, and 0.8 are compared. This effect is more accentuated at the leading edge (x/c=0.13), and disappears at x/c=0.25. The comparison at x/c=0.4 is missing in Fig.28 because it has been difficult to characterize the bubble from U records at this chord station when z/h=0.8.

Visualizations

The visualizations have been performed owing to the technique described above and sketched in Fig.2. As the laminar bubble of transition remains not so easy to characterize by visualization when α varies between 0deg and 12deg because of its size, the effort has been made to emphasize visualizations when the wing is stalled. The previous final report[1] has clearly shown what smoke visualization can do for the knowledge of dynamic stall behavior in a 2D configuration. In the present work, the flow at the 3D wing tip is dominated by strong vorticity, particularly at stall. It has seemed interesting to explore this region and to outline the investigation of the influence of the tip vortex on dynamic stall.

When the laser sheet illuminates a vertical plane at the trailing edge, the wing-tip vortex is visualized as shown in Fig.29. The vortex pattern obtained at three incidences (6deg, 12deg and 18deg) when the wing is at rest (right side of the figure) has been compared at same incidence when the wing oscillates (left side). It can be deduced from the pictures that the behavior of the wing–tip vortex is a quasi-steady one, at least in our experimental condition of oscillation k=0.188.

Concerning the flow on the upper side of the wing, it has been visualized using a horizontal laser sheet located successively at two different z/h=0.6 and 0.8. The dynamic stall has not been observed for incidences oscillating between 6deg and 18deg at either of z/h, as it is observed on 2D airfoils in the same incidences condition. The pictures of Fig.30 attest that the flow remains attached for each z/h at 16deg, due to the induced incidence generated by the downwash, as it has already been remarked from the U component profiles previously analyzed.

Nevertheless it has been possible to visualize the dynamic stall at higher incidence when α oscillates between 12deg and 24deg. The figure 31 shows that the flow remains attached at 12deg for each z/h and is separated at 20deg, proceeding from a leading edge bubble. It appears from the pictures taken at 20deg that the reattachment at the leading edge is more achieved closer to the tip (z/h=0.8) due to the nearness of the tip vortex. Nevertheless, the analysis of the different pictures taken at different incidences during the oscillation seem to indicate that the dynamic stall process in 3D configuration is very similar to 2D dynamic stall observed on 2D airfoils at lower incidence.

CONCLUSIONS

Two wings of NACA 0012 airfoil oscillating in pitch have been tested in 2D and 3D configurations at a Reynolds Numbers $Re=10^5$. The mean angles of attack were $\alpha_0=6$ and 12deg, the angular amplitude $\Delta\alpha=\pm6$deg and the frequency oscillation k=0.188.

Smoke filaments emitted from upstream allowed the flow visualization on the upper side of the airfoil, illuminated by a laser sheet. In the 3D case, wing-tip vortex pictures taken in a vertical plane containing the trailing edge have complemented visualizations. Pictures of the flowfield were shot at different instants of the oscillation by use of a numerical camera and movies were realized from the pictures. An higher mean angle of incidence $\alpha_0=18$deg has been used to visualize the dynamic stall.

Measurements of the velocity components were performed using an embedded laser velocimeter allowing the 3 components measurement in 3D configuration. The velocity survey was made normally to the airfoil surface, from 100mm outside to 0.2mm to the wall at three chord stations. The turbulence intensities and the Reynolds stresses were deduced for given phases of the oscillation from about 200 samples of the velocity components statistically analyzed. The analysis of velocity and turbulence components has underlined the influence of the wing-tip vortex on the boundary layer transition and separation mainly due to the decrease of the effective incidence induced by the downwash. It has thus been possible to quantitatively characterize a separation bubble close to the leading edge when the wing oscillates at low incidence (less than 12deg), like it has already been found in the 2D case[1]. The bubble remains located at about the middle front part of the upperside with a maximal thickness Y/C less than 1.5%. It is observed that the bubble is thicker during downstroke than during upstroke as in 2D configuration[1]. The bubble thickness decreases close to the tip where the effective incidence is lower than in the inboard region (wing-tip vortex effect).

The different features of the flow around the oscillating airfoil during 3D dynamic stall have been analyzed both from velocity measurements and visualizations. It can be concluded that although dynamic stall occurs at higher incidence than in 2D configuration due to the induced incidence, the process of separation and reattachment appears to be the same than in 2D configuration.

This study has clearly shown that embedded laser velocimetry is a suitable and useful tool to investigate unsteady boundary layer and dynamic stall regime occurring on oscillating airfoils even in 3D configuration. Moreover, these results on velocity and turbulence in 3D boundary layer have been constituted in a data base that will be very useful in computational unsteady boundary layer.

REFERENCES

1. C. Maresca, E. Berton, D. Favier, “Embedded LDV Measurements in the Boundary Layer of Moving Walls” Final Technical report, ERO Contract n° N 68171-99-M-6670, December 2000.

2. W. J. McCroskey, K. W. McAlister, L. W. Carr, and S. L. Pucci, “An Experimental Study of Dynamic Stall on advanced Airfoils sections Volume 1. Summary of Experiments”,
NASA TM 84245, July 1982.

3. K. W. McAlister, S. L. Pucci, W. J. McCroskey, and, L. W. Carr, “An Experimental Study of Dynamic Stall on advanced Airfoils sections Volume 2.Pressure and Force Data”
NASA TM 84245, September 1982.

4. L. W. Carr, W. J. McCroskey, K. W. McAlister, S. L. Pucci, and O. Lambert, “An Experimental Study of Dynamic Stall on advanced Airfoils sections Volume 3.Hot wire and hot film measurements ”
NASA TM 84245, December 1982.

5. C. Maresca, D. Favier, and J. Rebont, “Unsteady Aerodynamics of an Airfoil at High Angle of Attack Performing Various Linerar oscillations in Uniform Stream.”
Journal of American Helicopter society, Vol.20, n°7, pp. 865-871, 1982

6. D. Favier, A. Agnes, C. Barbi, and C. Maresca, “The combined Translation-Pitch Motion of a New Airfoil Dynamic Stall Simulation”,
Journal of Aircraft, Vol.25n° 9, pp. 805-814, 1988.

7. E. Berton, D.Favier, C.Maresca, “Embedded L.V. methodology for boundary-layer measurements on oscillating models”, A.I.A.A., Proceedings of the 28th Fluid Dynamics Conf., A.I.A.A. paper n° 97/1832, Snowmass, June 1997.

8. W. G. Bouseman, « Evaluation of Airfoil Dynamic Stall Characteristics for Maneuverability", 26th European Rotorcraft Forum, The Hague, Netherland, September 26-29, 2000.

9. K. Pahlke, E. Chelli, "Calculation of Multibladed Rotors in Forward Flight Using 3D Navier-Stokes Method", Proceedings of the 26TH European Rotorcraft Forum, 26-29 September 2000, The Hague, The Netherlands.

10. D.Favier, C.Maresca, M. Nsi Mba, E. Berton, A.Agnes, "New Type of Embedded Laser Doppler Velocimeter (ELDV) for Measurement of Rotary Wings Boundary-Layer", The Review of Scientific Instruments, Vol. 66, n° 6, pp. 2447-2455, 1997.

S2 LUMINY

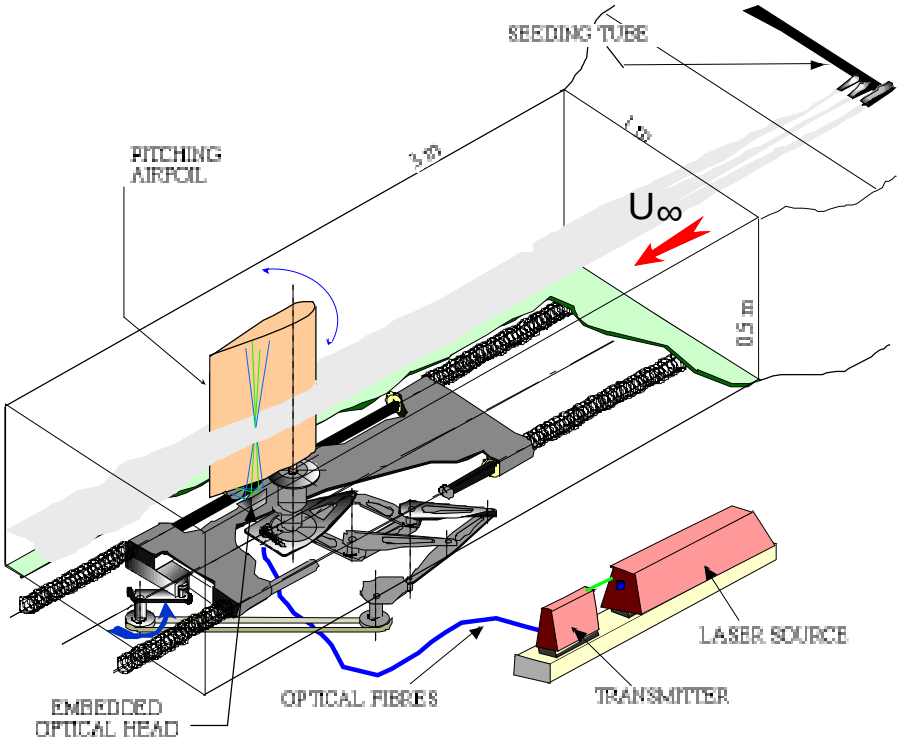

Fig 1

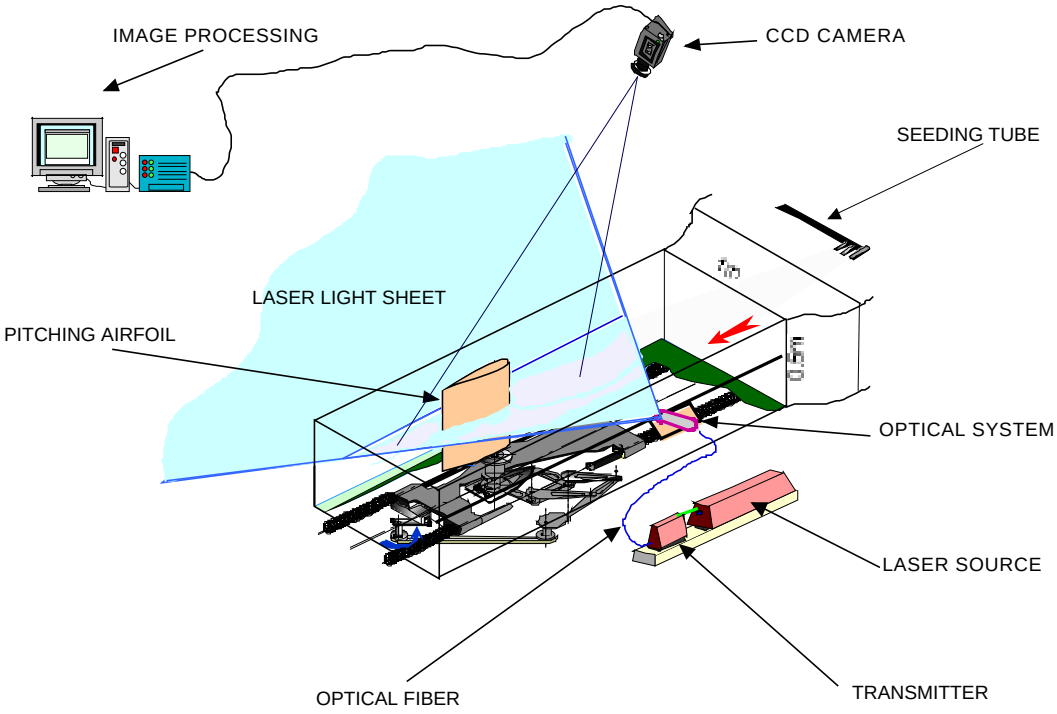

VISUALIZATION IN S2L

Fig 1

Fig3

2D velocity measurement

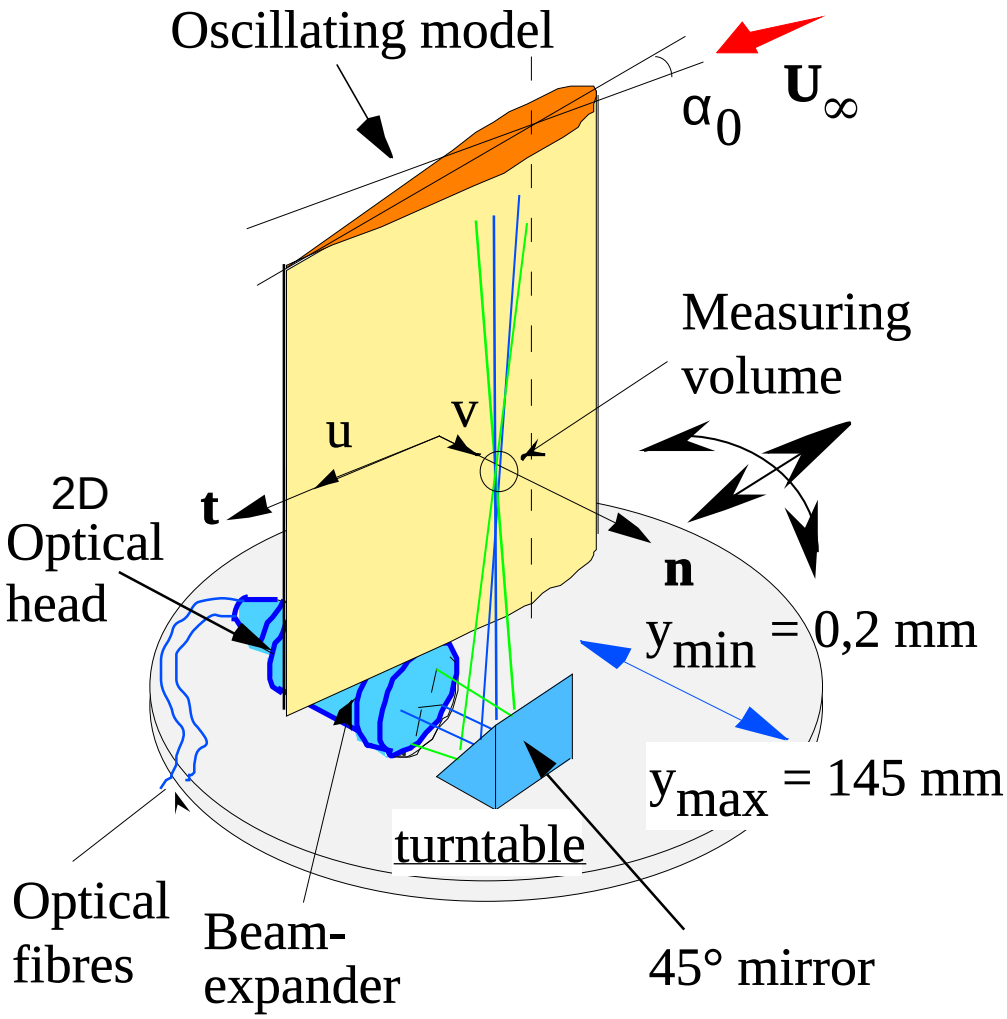

Fig 4

3D velocity measurement

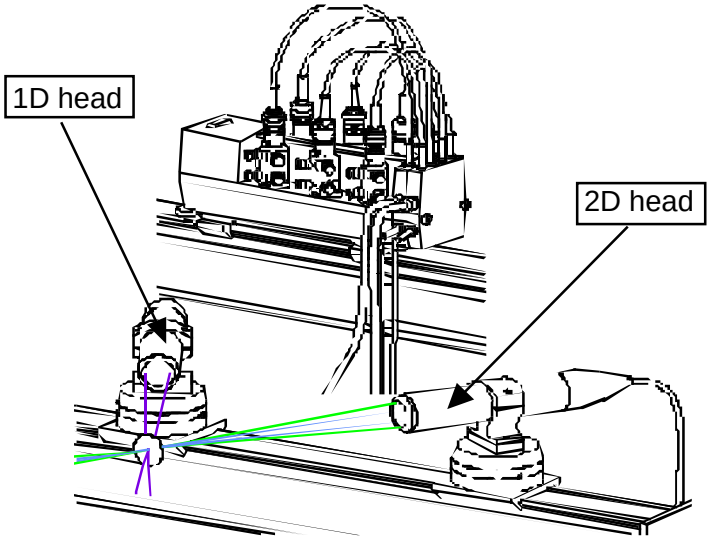

3D LDA

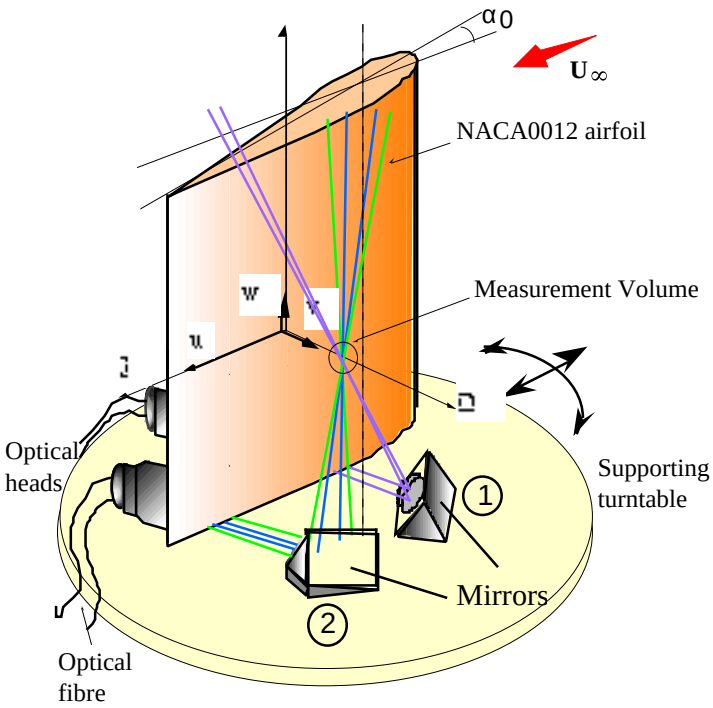

Embedded 3D LDA

Fig5

VELOCITY COMPONENTS

VERTICAL PLANE: Green and Purple beams

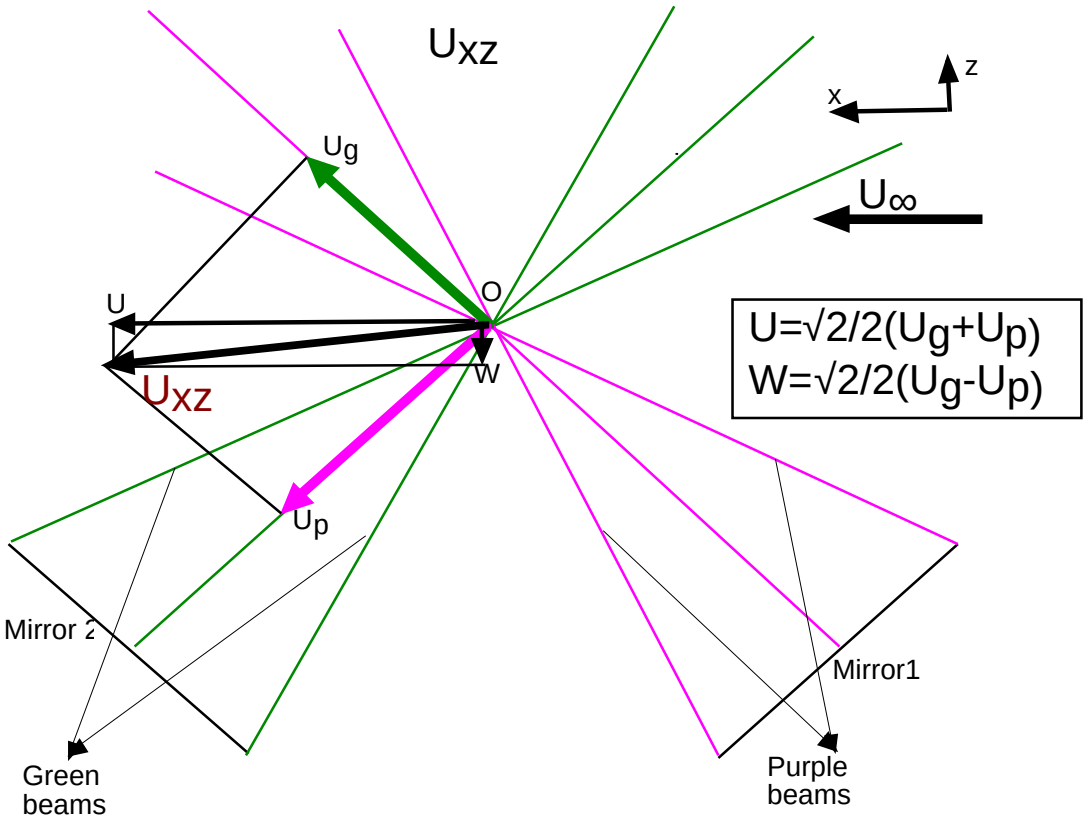

$U=\sqrt{2}/2(U_g+U_p)$
$W=\sqrt{2}/2(U_g-U_p)$

Blue beams

$V=U_b$

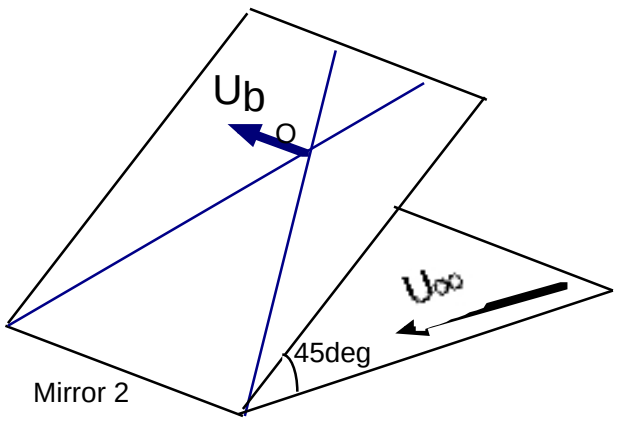

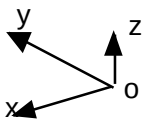

ox chordwise: U
oy normal : V
oz spanwise : W

Fig6

Effect of tip wing on the steady boundary layer
Velocity components and turbulence at
x/c=0.25, α=0deg

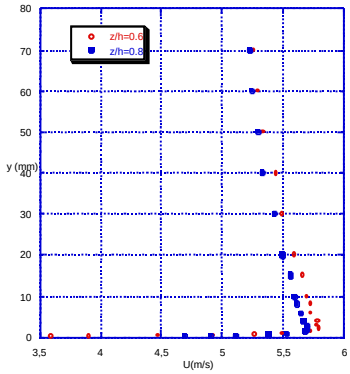

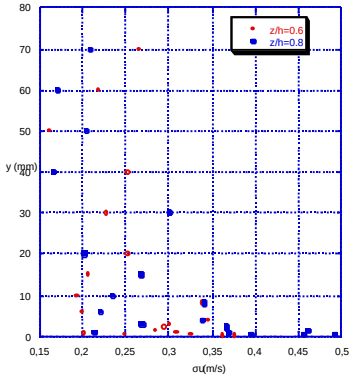

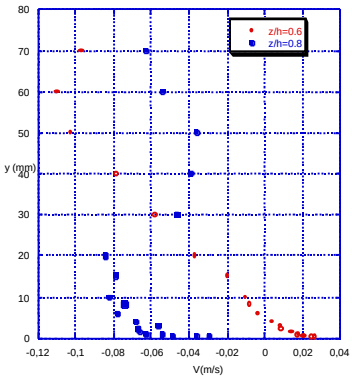

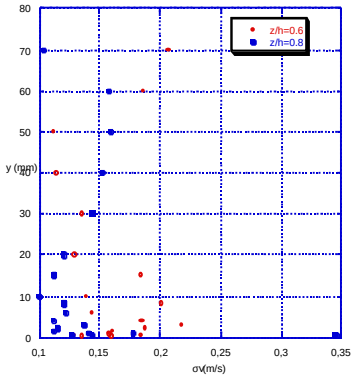

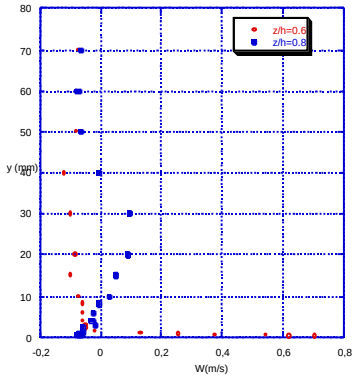

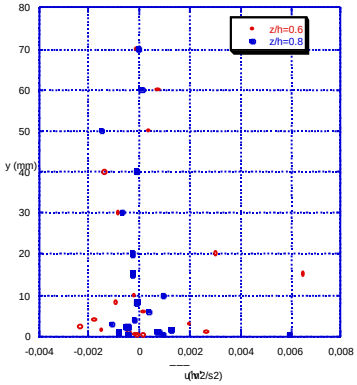

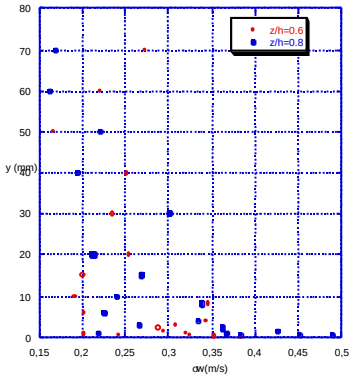

Effect of tip wing on the steady boundary layer
Velocity components and turbulence at x/c=0.25, α=6deg

Fig7

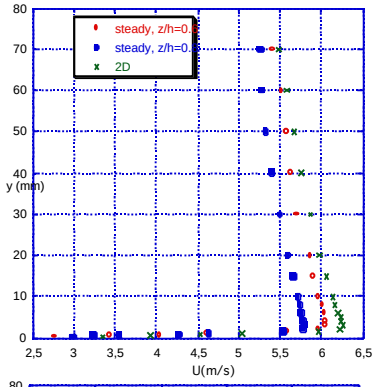

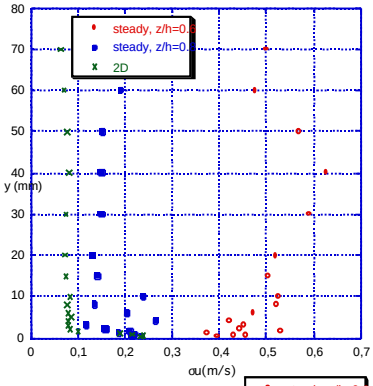

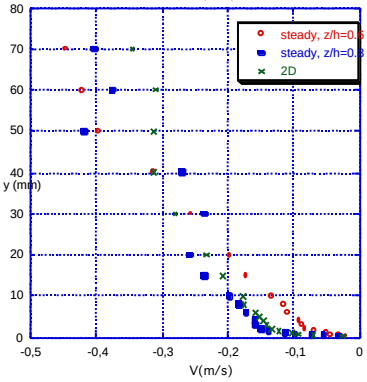

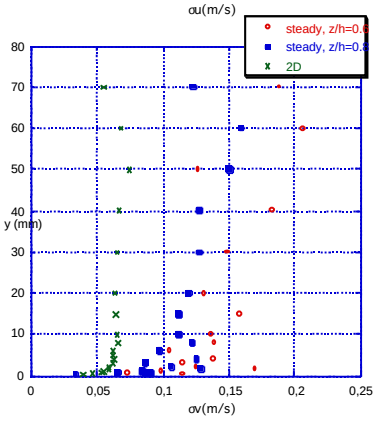

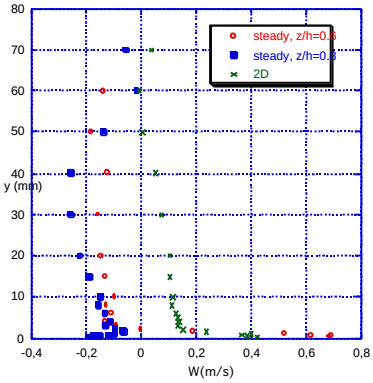

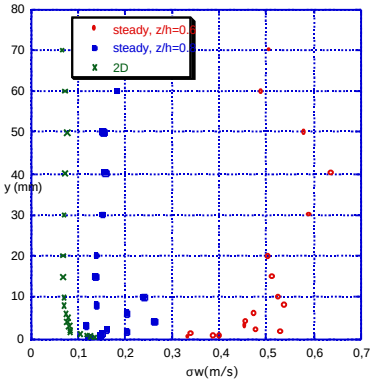

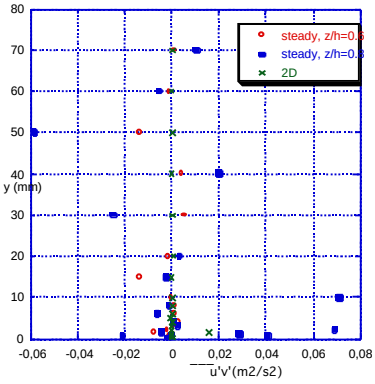

Effect of tip wing on the steady boundary layer
Velocity components and turbulence at x/c=0.25, α=12deg

Fig8

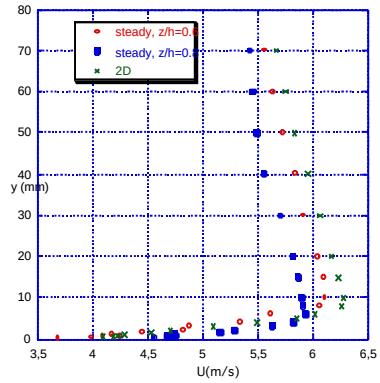

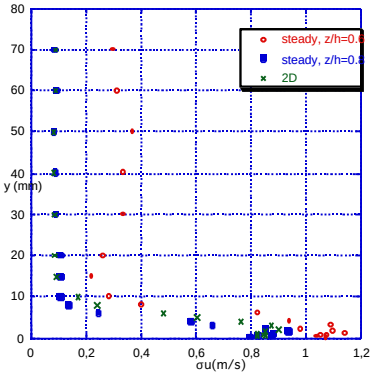

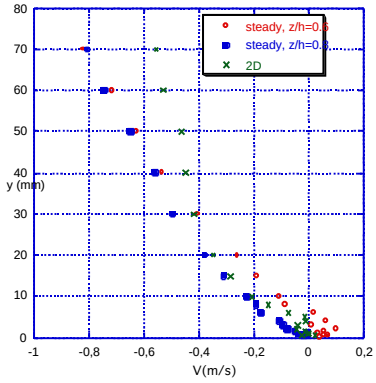

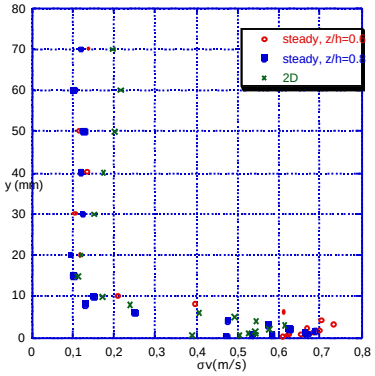

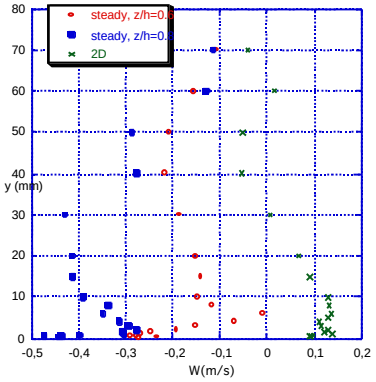

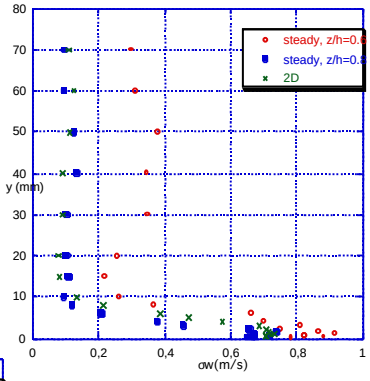

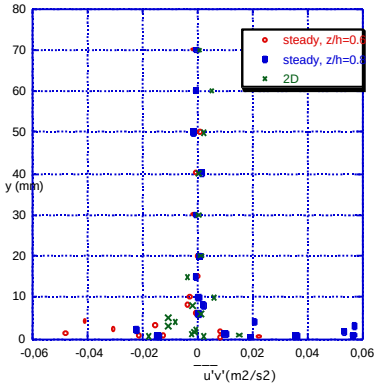

Effect of tip wing on the steady boundary layer
Velocity components and turbulence at x/c=0.25, α=18deg

Fig9

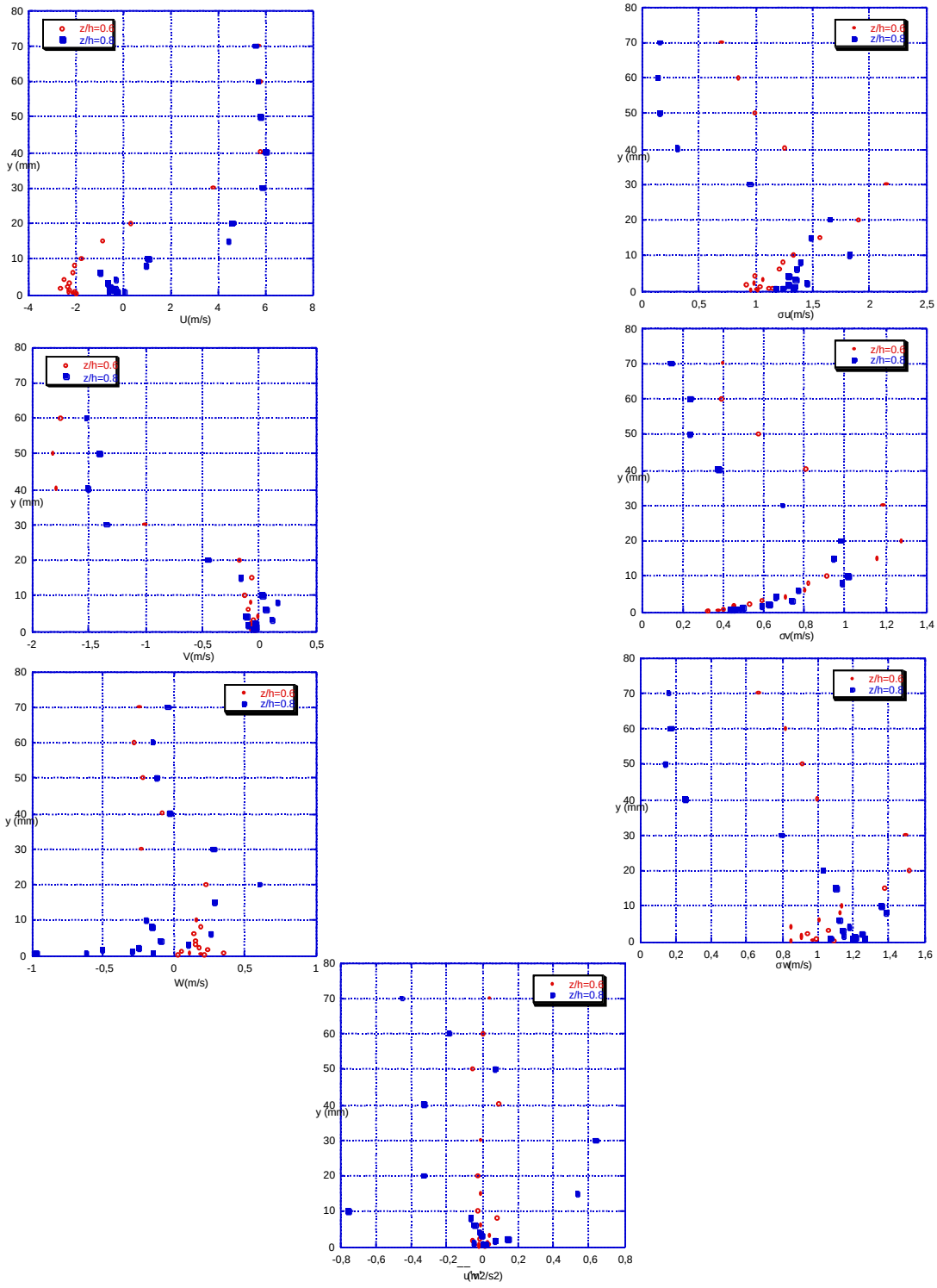

Effect of tip wing
on the velocity components at x/c=0.25,
α_0=6deg,$\Delta\alpha$=6deg

Fig10

α=0

α=12

U component

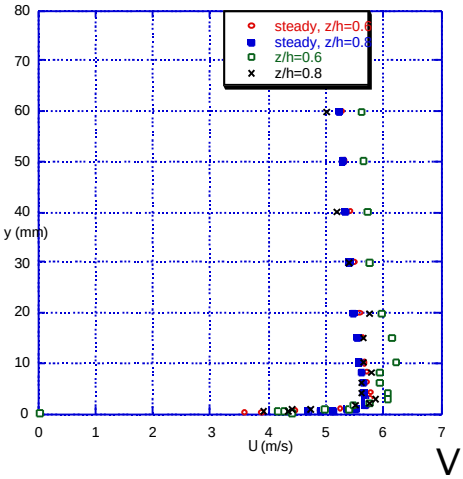

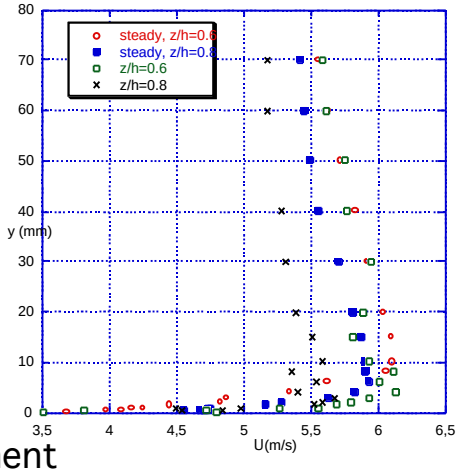

V component

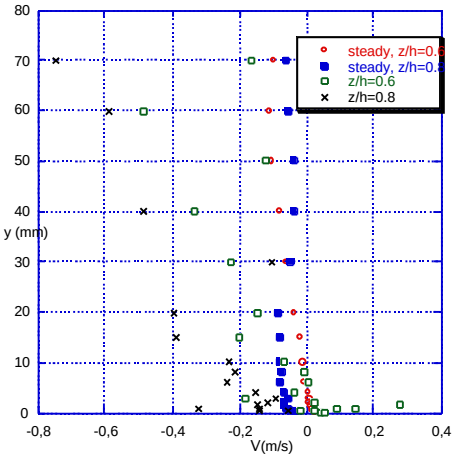

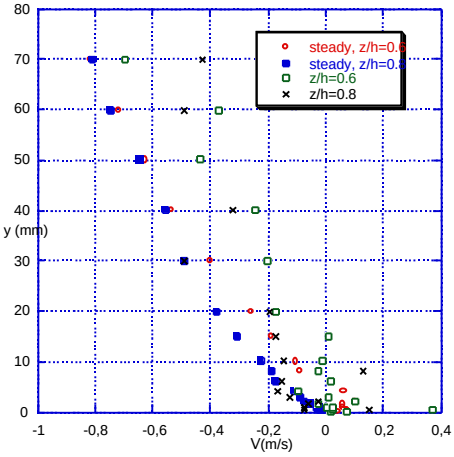

W component

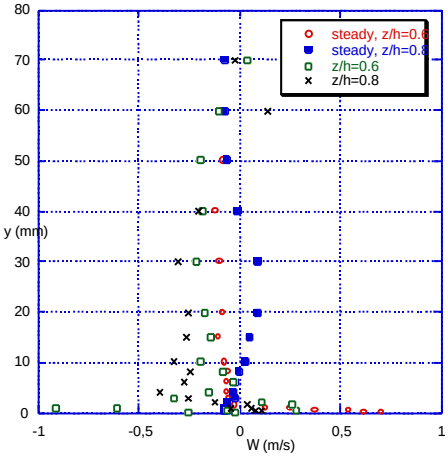

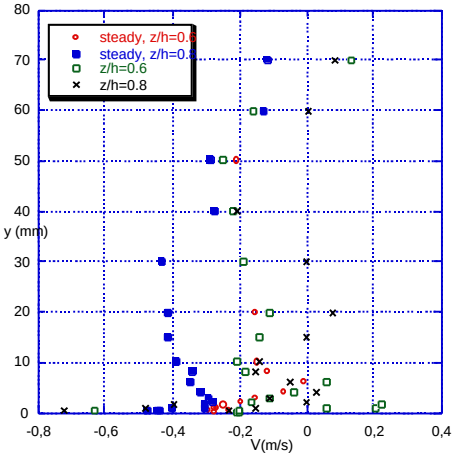

Effect of tip wing
on the turbulence at x/c=0.25,
α_0=6deg,$\Delta\alpha$=6deg

Fig11

α=0

α=12

σu

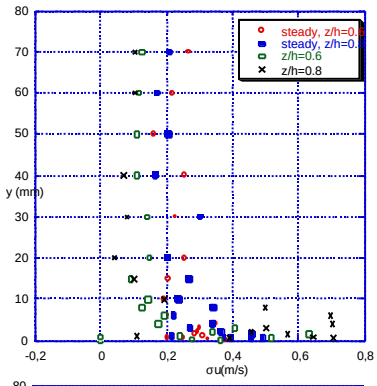

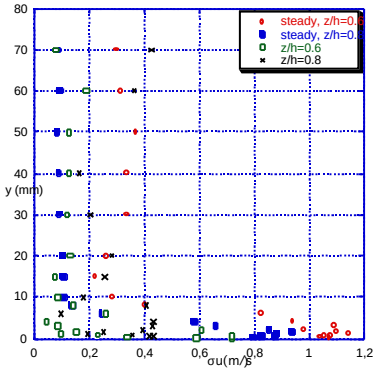

σv

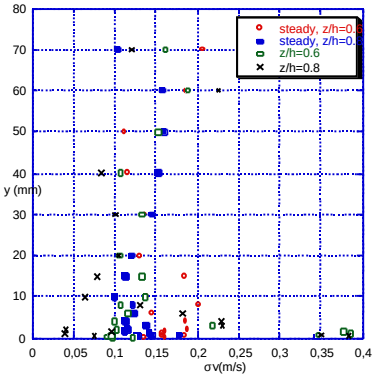

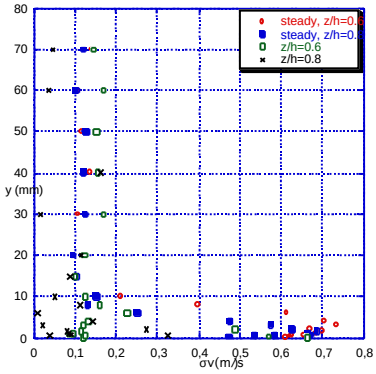

σw

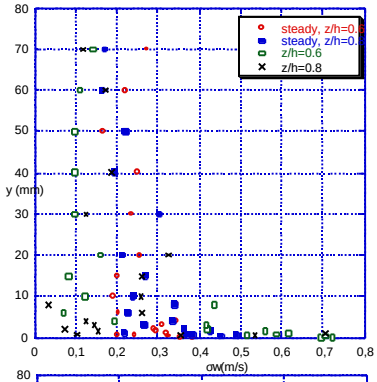

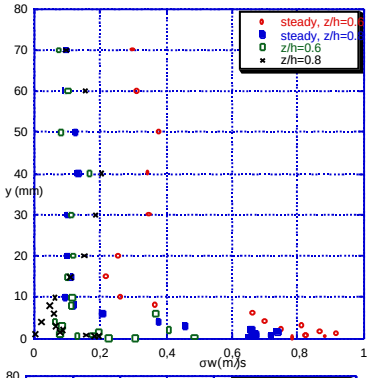

$\overline{u'v'}$

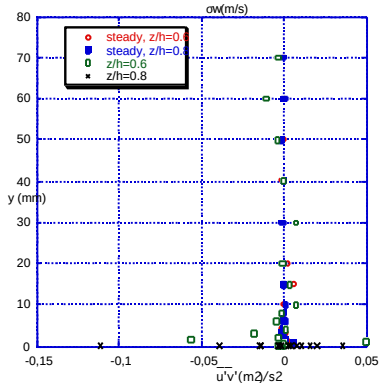

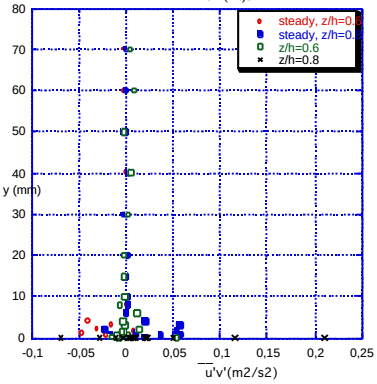

Effect of tip wing
on the velocity components at x/c=0.25,
α_0=6deg,$\Delta\alpha$=6deg

Fig12

α=6up

α=6down

U component

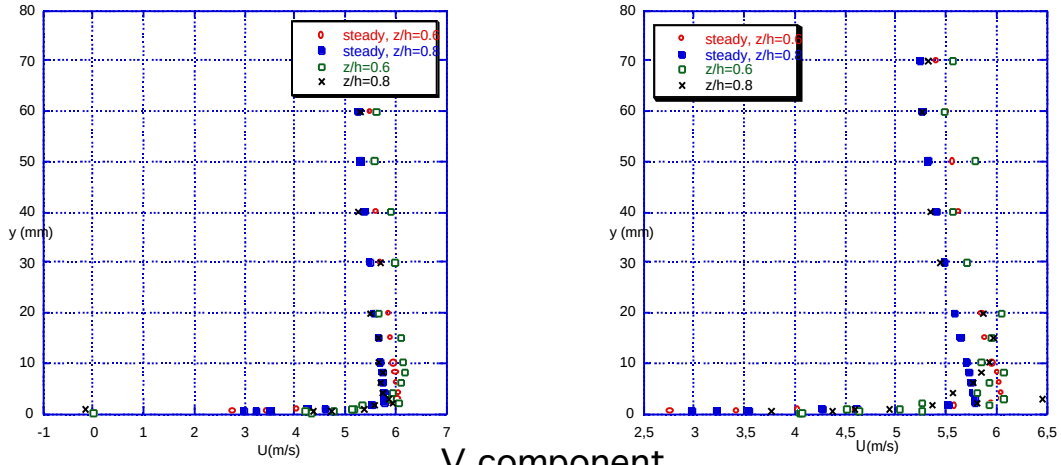

V component

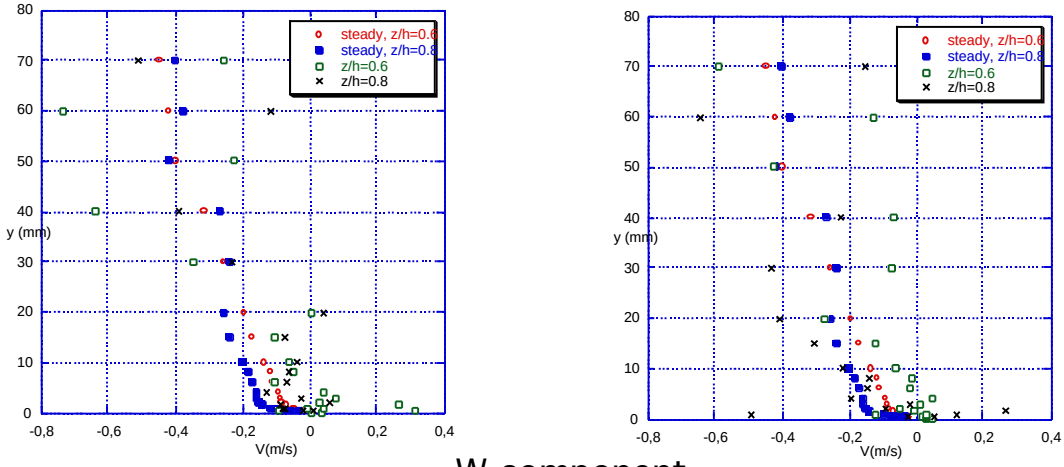

W component

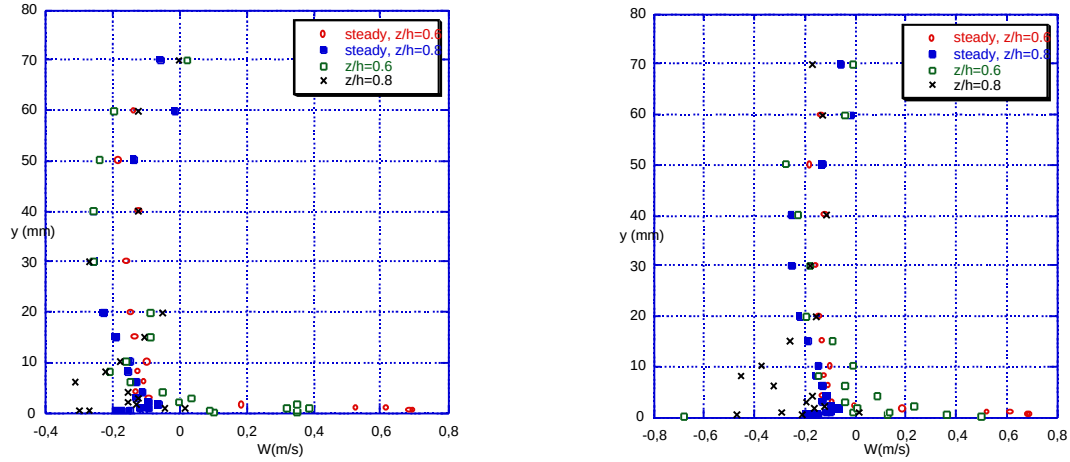

Effect of tip wing
on the turbulence at x/c=0.25,
α_0=6deg,$\Delta\alpha$=6deg

Fig13

α=6 up

α=6 down

σu

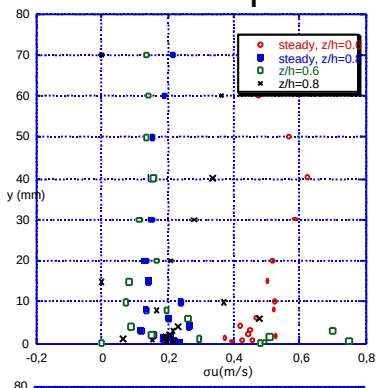

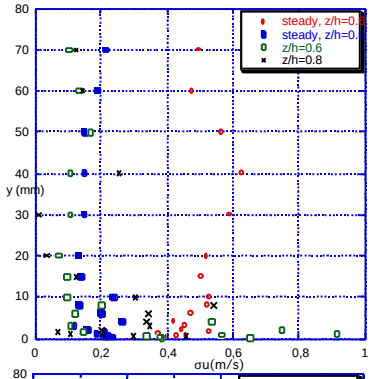

σv

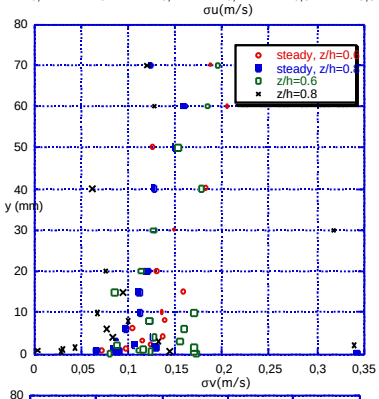

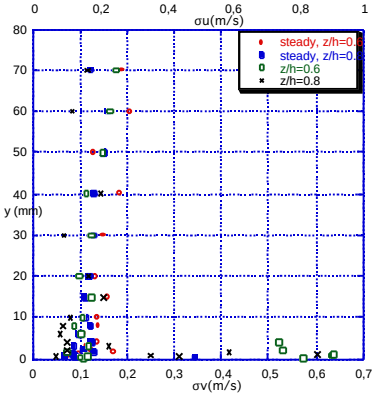

σw

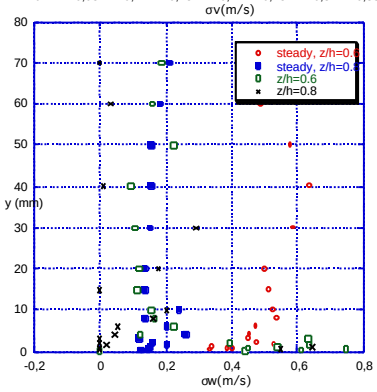

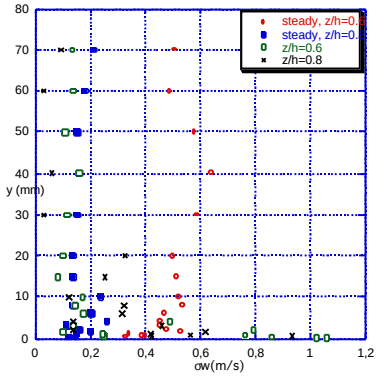

$\overline{u'v'}$

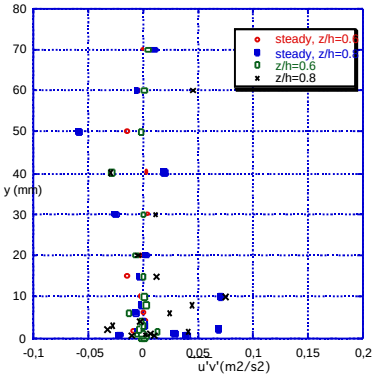

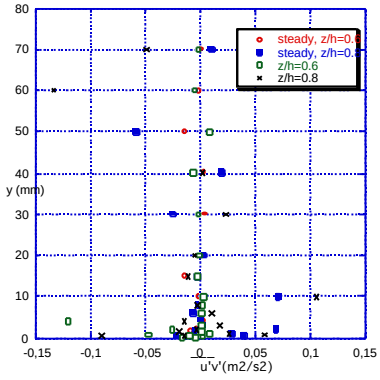

Fig14

Effect of tip wing on the velocity components at x/c=0.25, α_0=12deg, $\Delta\alpha$=6deg

α=6 α=18

U component

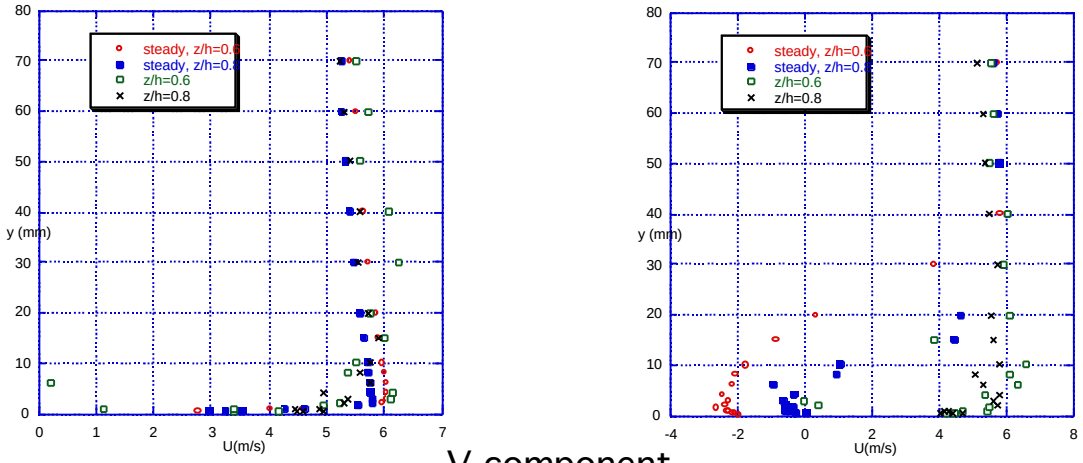

V component

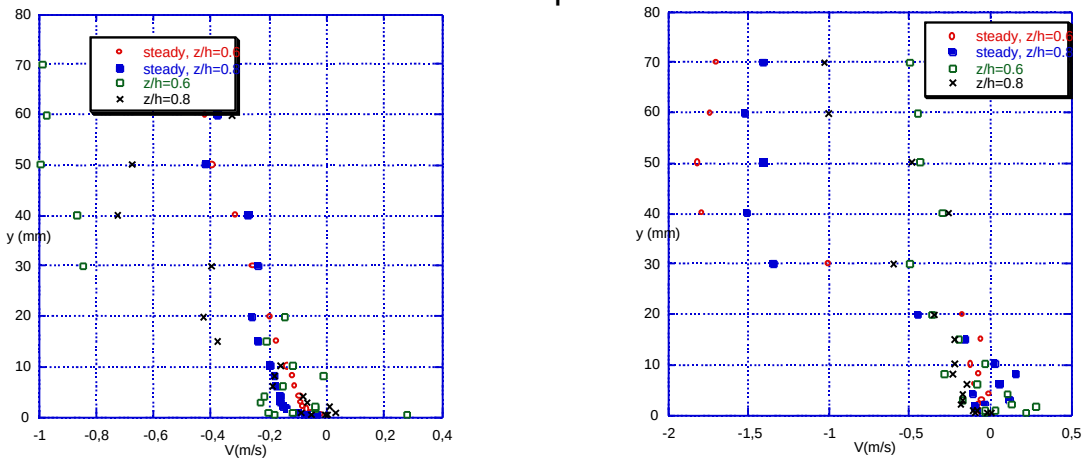

W component

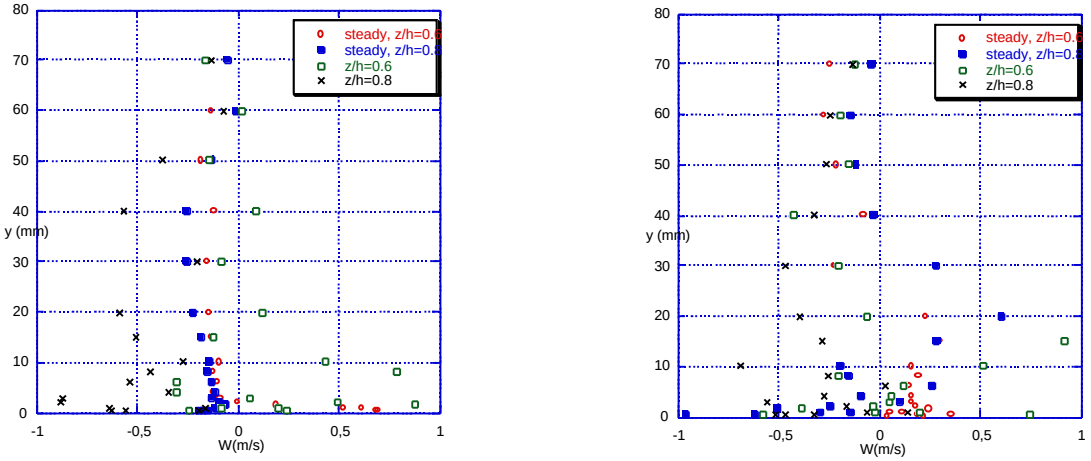

Effect of tip wing
on the turbulence at x/c=0.25,
α_0=12deg,Δα=6deg

Fig15

α= 6

α=18

σu

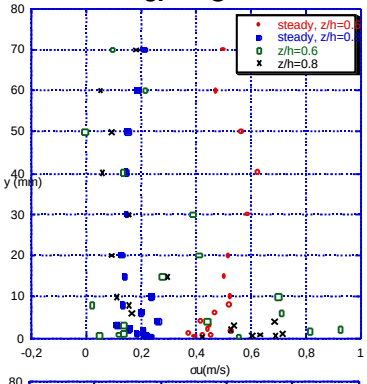

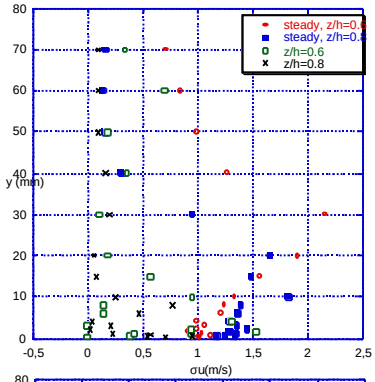

σv

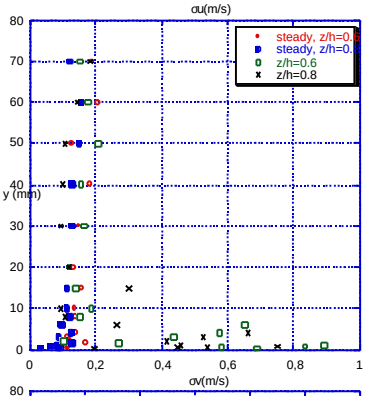

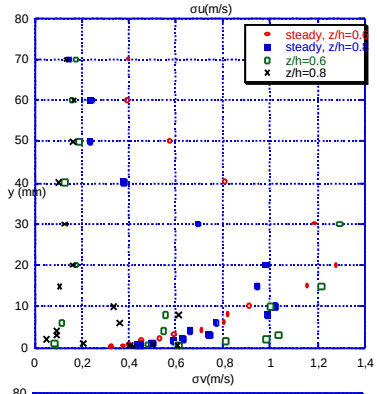

σw

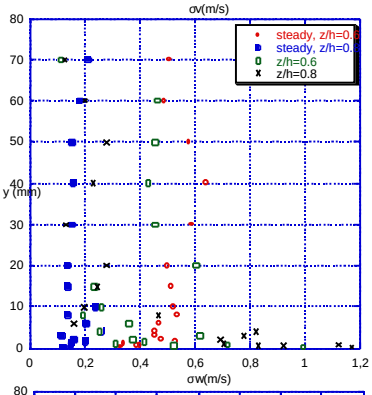

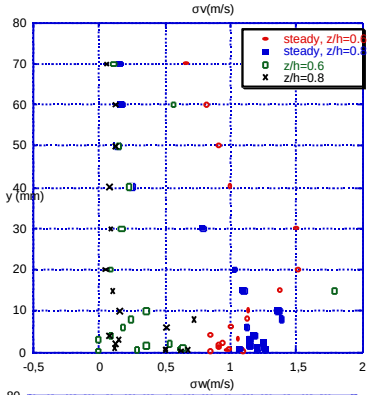

$\overline{u'v'}$

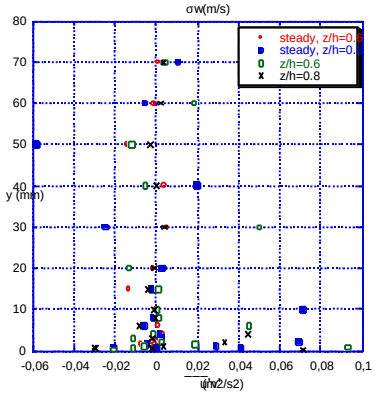

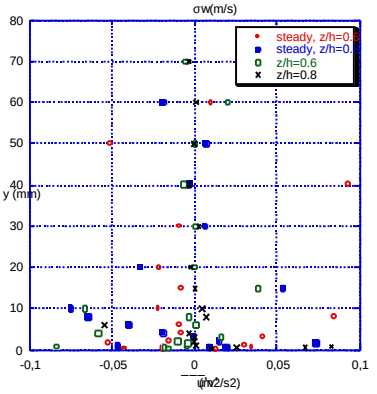

Effect of tip wing
on the velocity components at x/c=0.25,
α_0=12deg, $\Delta\alpha$=6deg

Fig16

α=12 up

α=12 down

U component

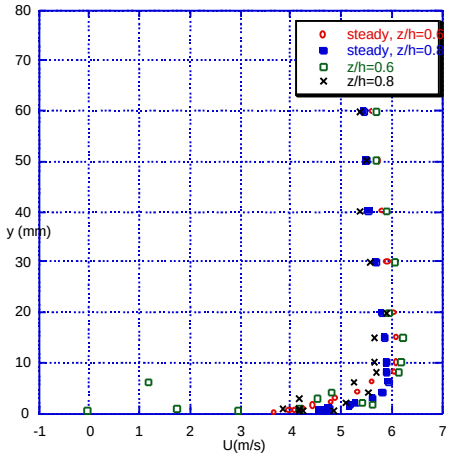

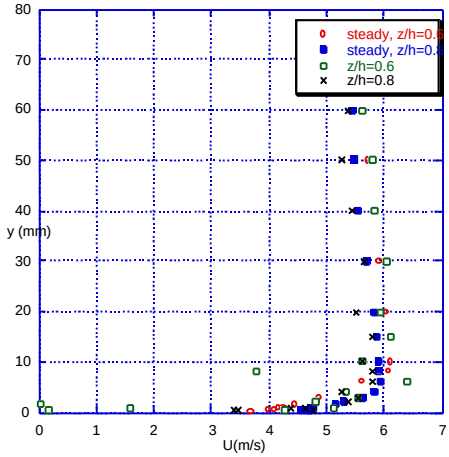

V component

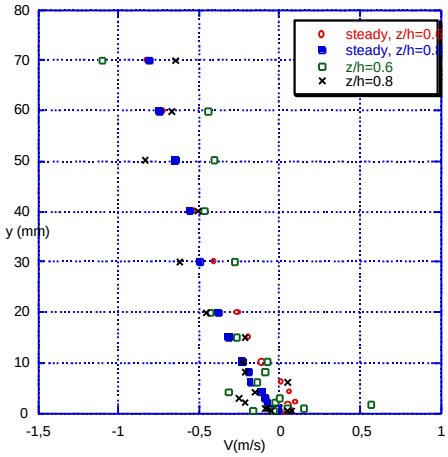

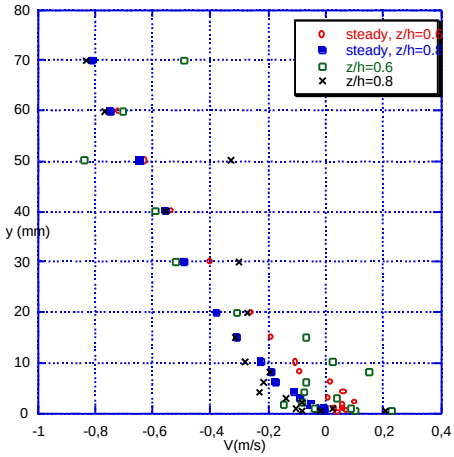

W component

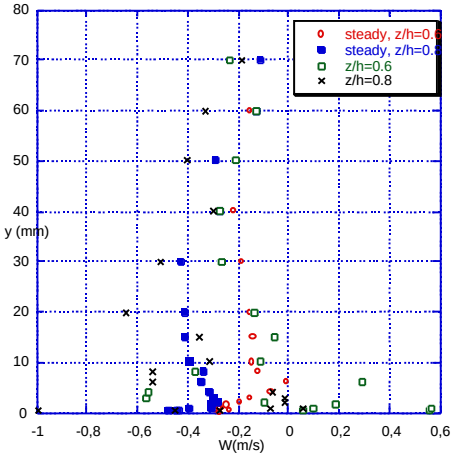

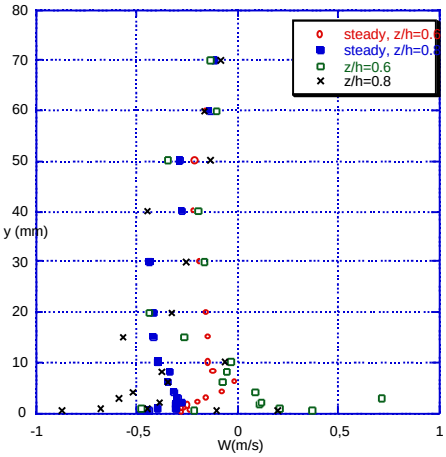

Effect of tip wing
on the turbulence at x/c=0.25,
α_0=12deg,$\Delta\alpha$=6deg

Fig17

α= 12 up

α=12 down

σu

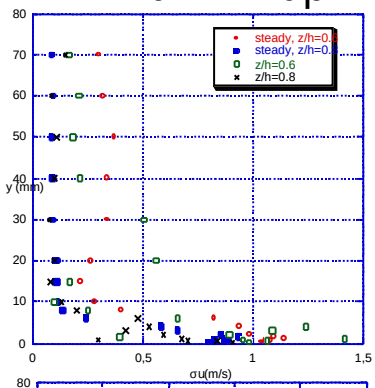

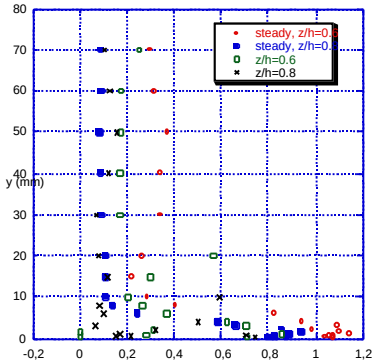

σv

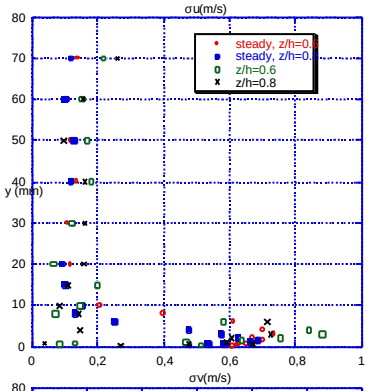

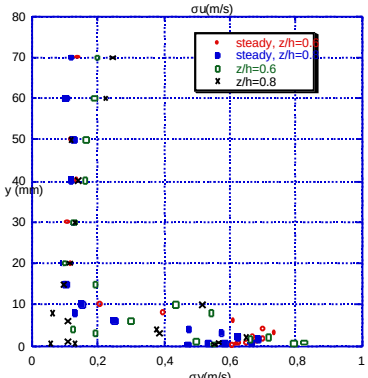

σw

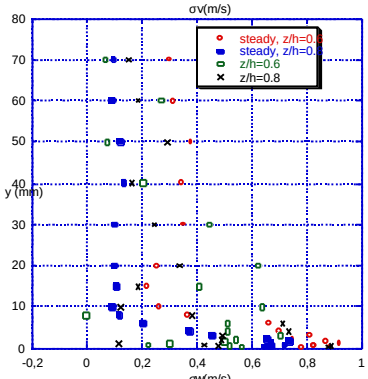

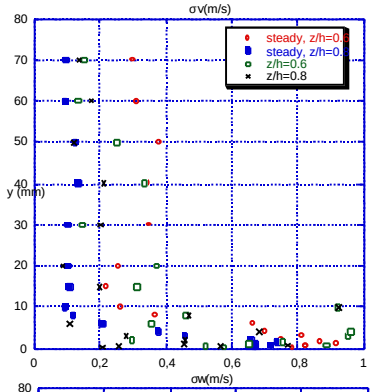

$\overline{u'v'}$

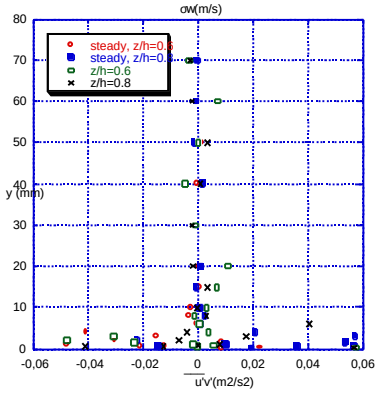

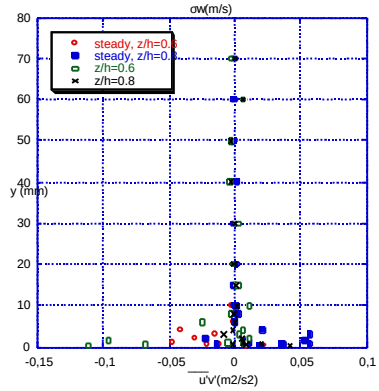

Effect of tip wing on the steady boundary layer
Velocity components and turbulence at x/c=0.25, α=6deg

Fig18

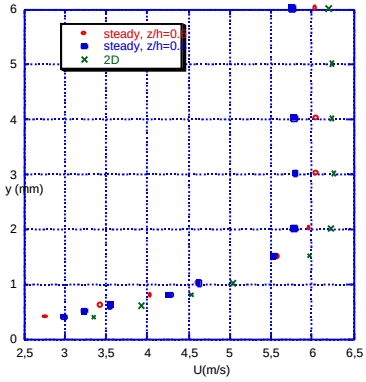

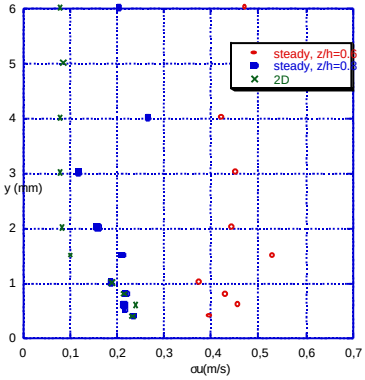

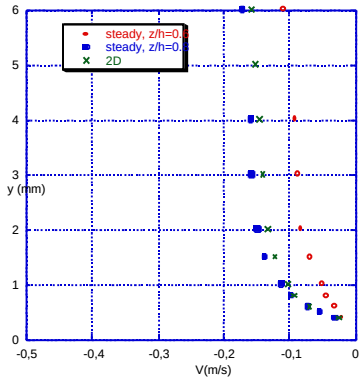

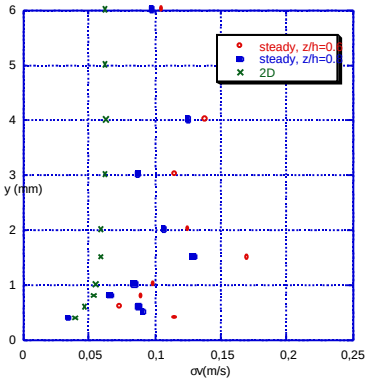

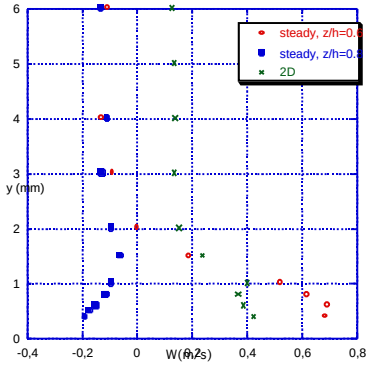

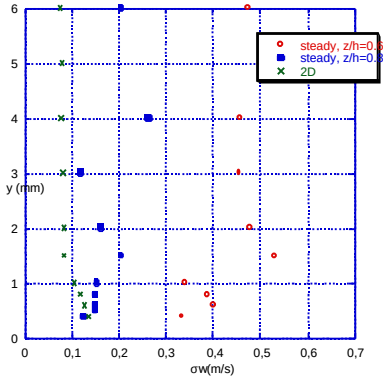

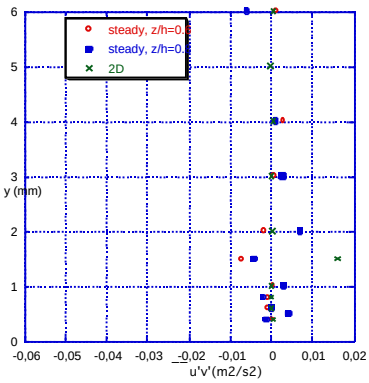

Effect of tip wing on the steady boundary layer
Velocity components and turbulence at x/c=0.25, α=18deg

Fig19

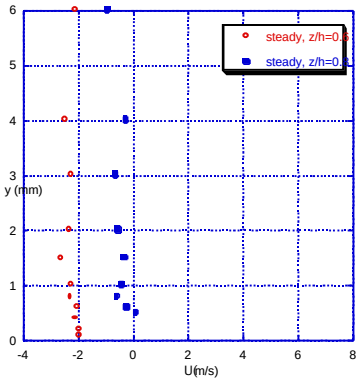

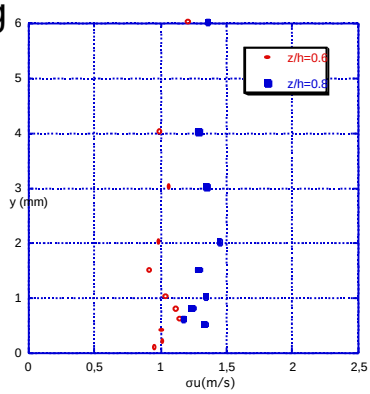

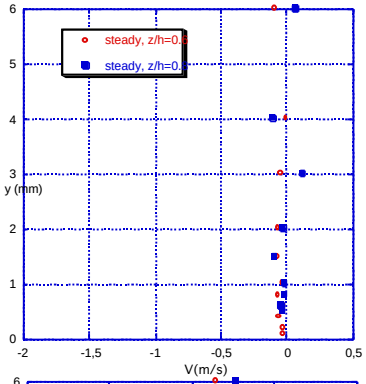

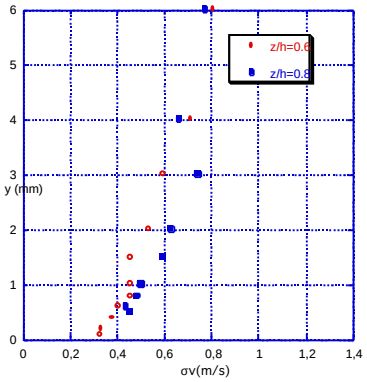

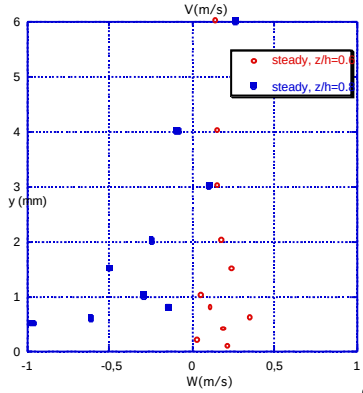

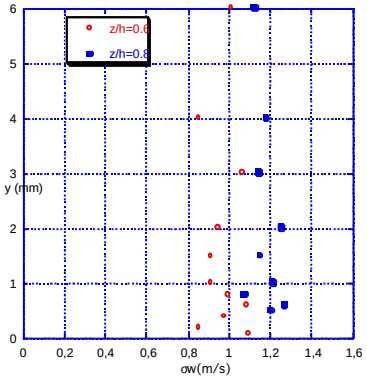

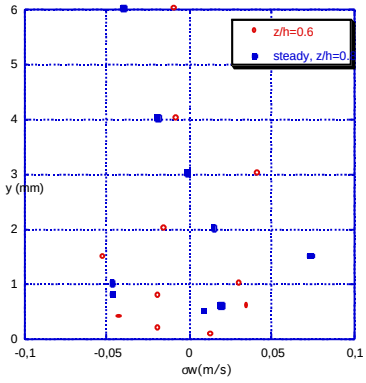

Fig20

Effect of tip wing on the velocity components at x/c=0.25, α_0=6deg,$\Delta\alpha$=6deg

α=6up

α=6down

U component

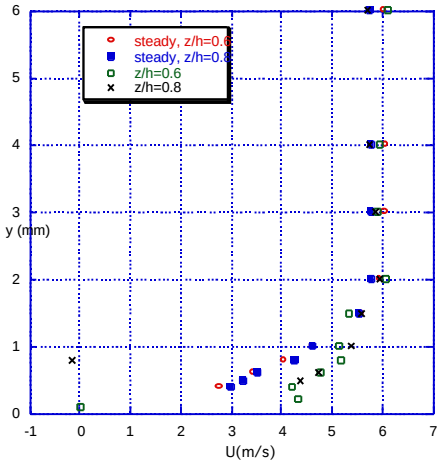

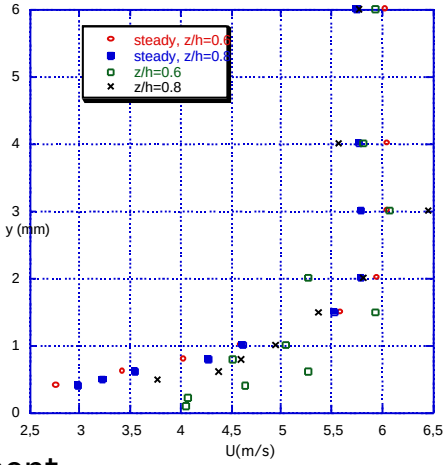

V component

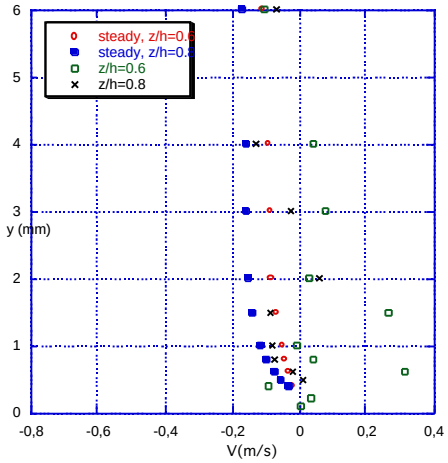

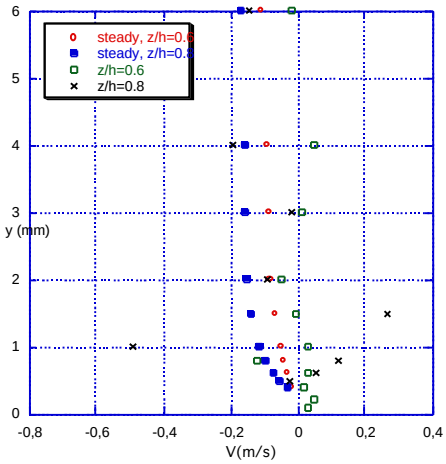

W component

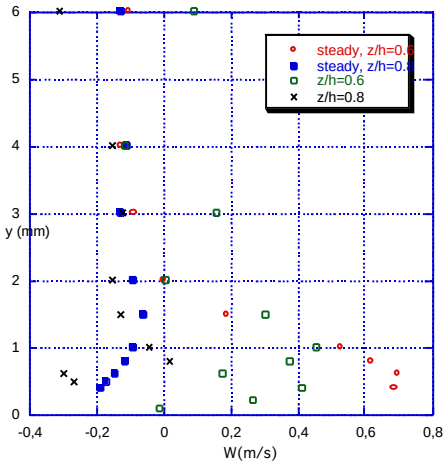

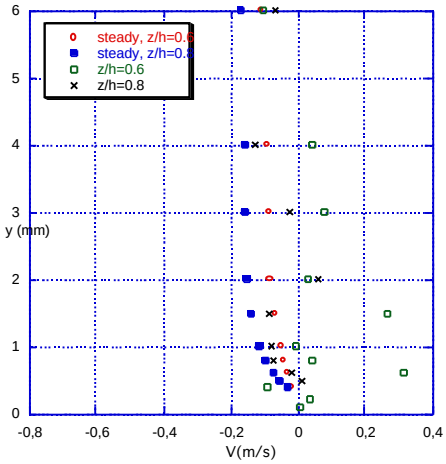

Effect of tip wing
on the turbulence at x/c=0.25,
α_0=6deg,$\Delta\alpha$=6deg

Fig21

α=6 up

α=6 down

σu

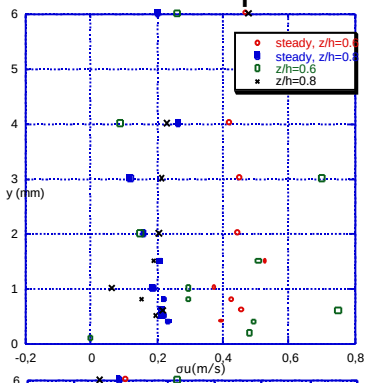

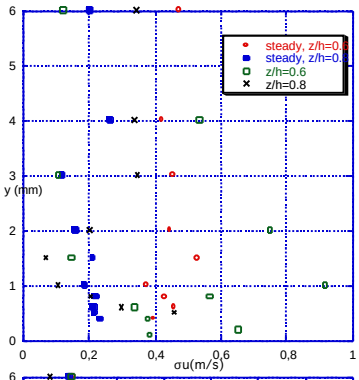

σv

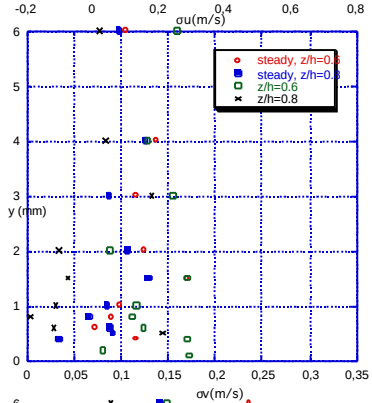

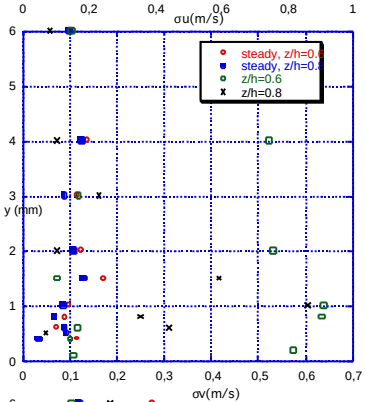

σw

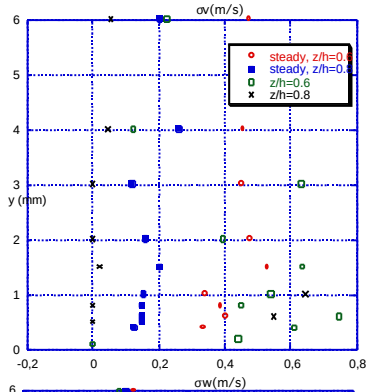

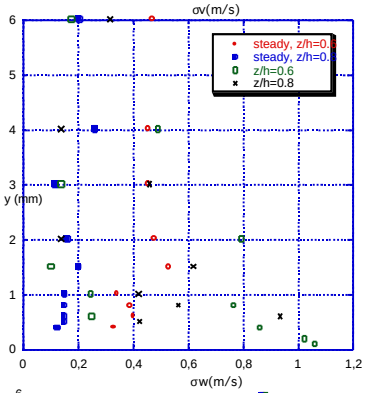

$\overline{u'v'}$

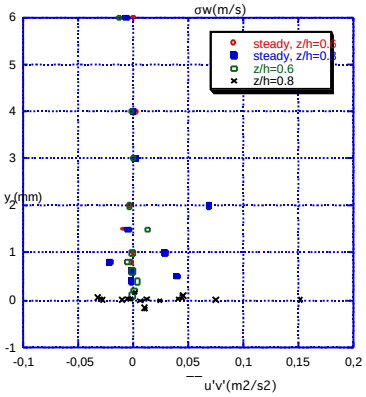

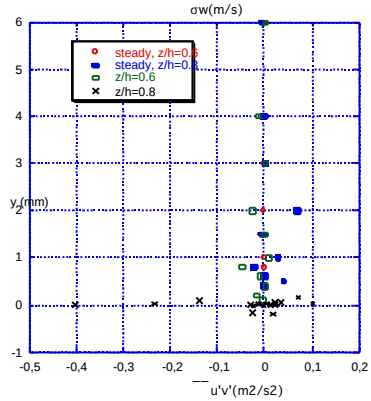

Effect of tip wing
on the velocity components at x/c=0.25,
α_0=12deg, $\Delta\alpha$=6deg

Fig22

α=6

α=18

U component

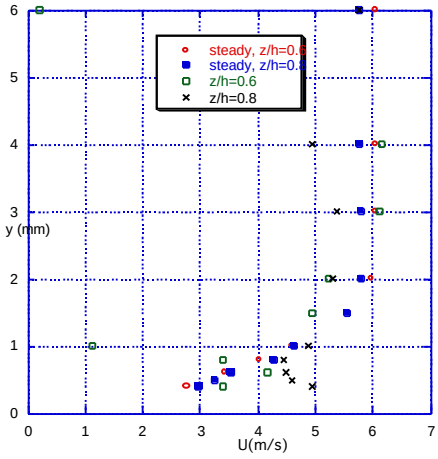

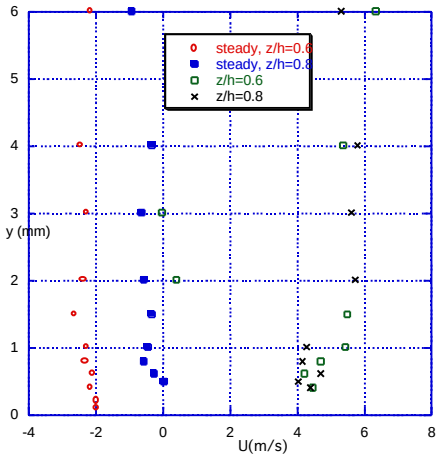

V component

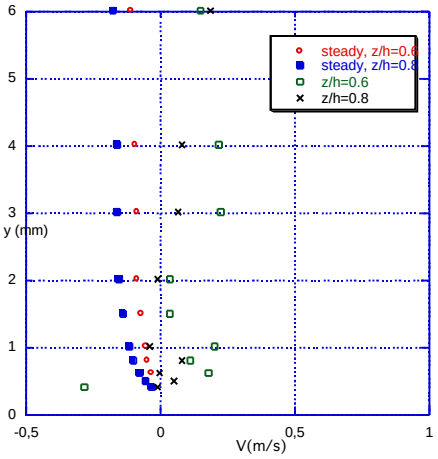

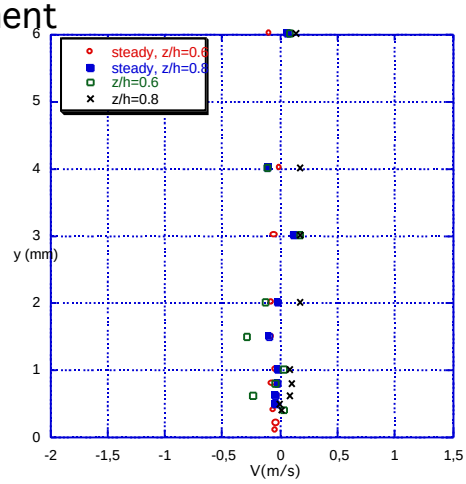

W component

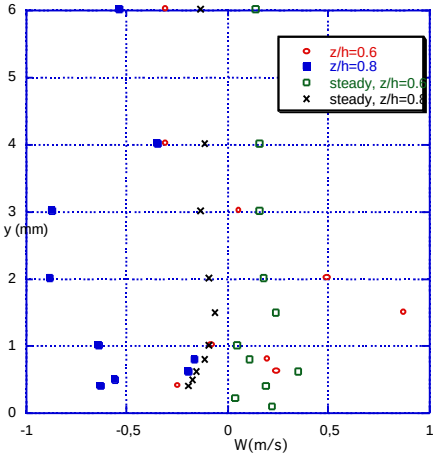

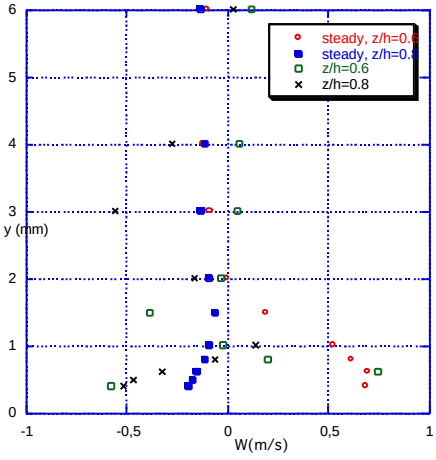

Effect of tip wing
on the turbulence at x/c=0.25,
α_0=12deg,Δα=6deg

Fig23

α= 6

α=18

σu

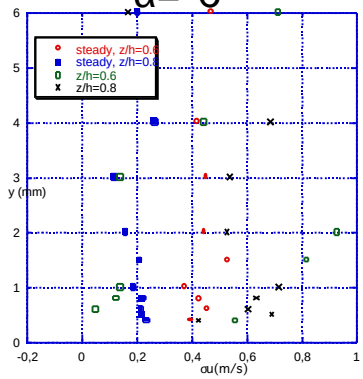

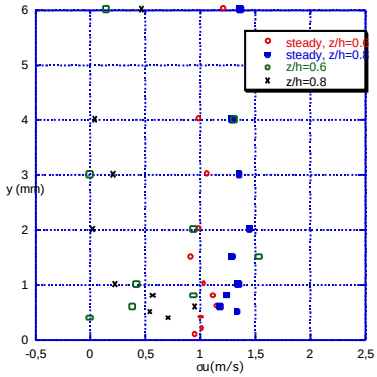

σv

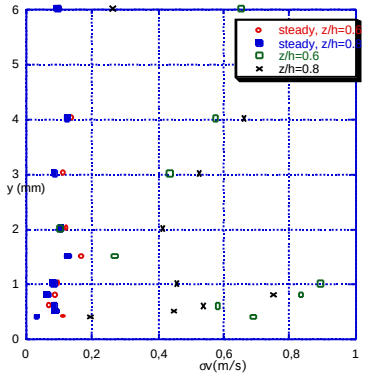

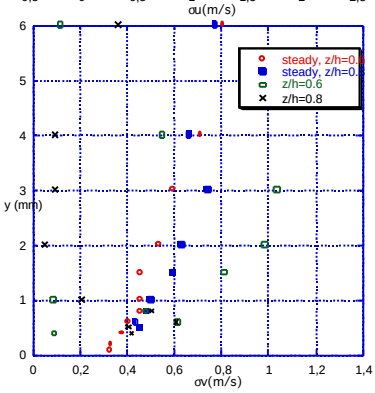

σw

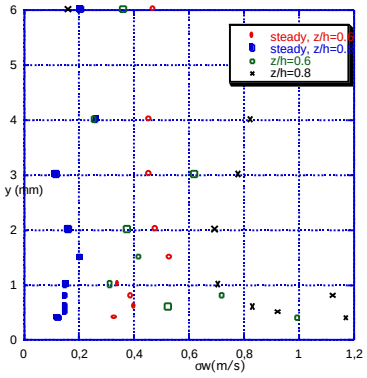

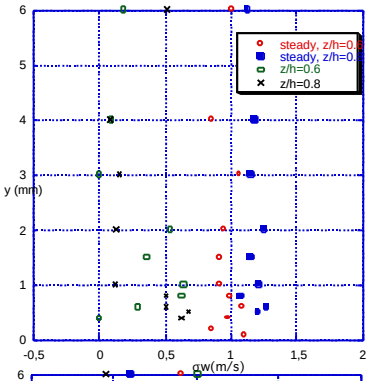

$\overline{u'v'}$

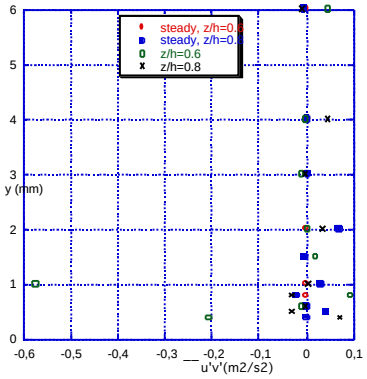

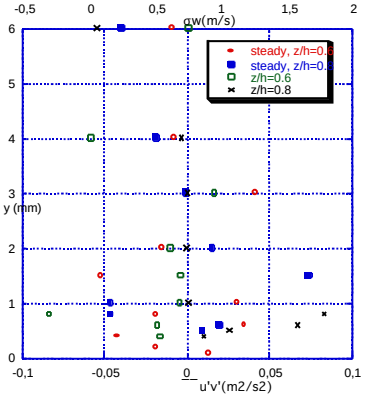

Fig 24

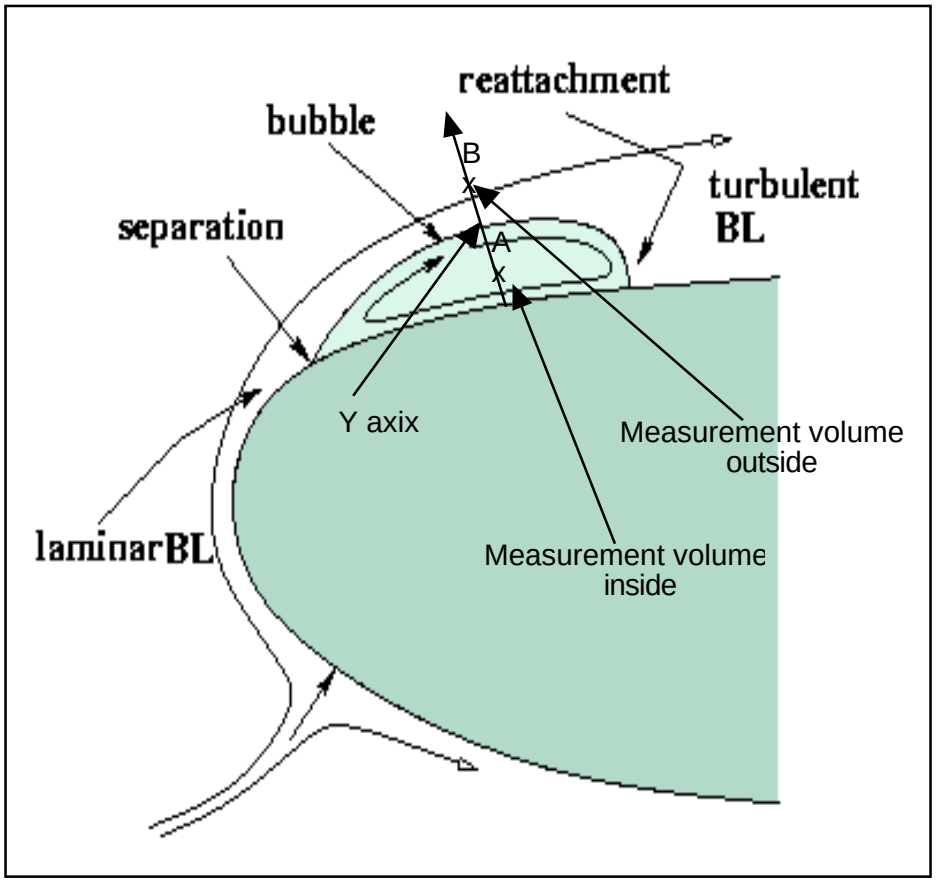
reattachment
bubble
B
turbulent
BL
separation
A
Y axix
Measurement volume
outside
laminarBL
Measurement volume
inside

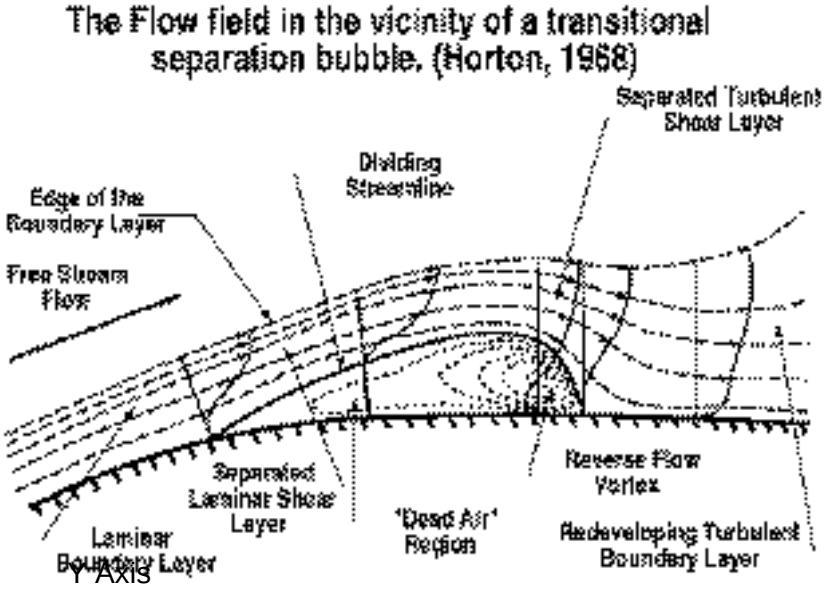
The Flow field in the vicinity of a transitional separation bubble. (Horton, 1968)
Separated Turbulent Shear Layer
Dividing Streamline
Edge of the Boundary Layer
Free Stream Flow
Separated Laminar Shear Layer
Reverse Flow Vortex
Laminar Boundary Layer
'Dead Air' Region
Redeveloping Turbulent Boundary Layer
Y Axis

Fig 25

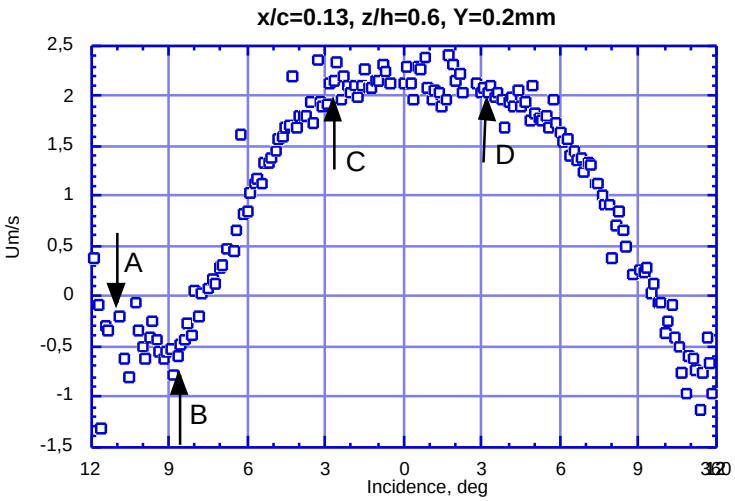
x/c=0.13, z/h=0.6, Y=0.2mm
Um/s
Incidence, deg
A
B
C
D

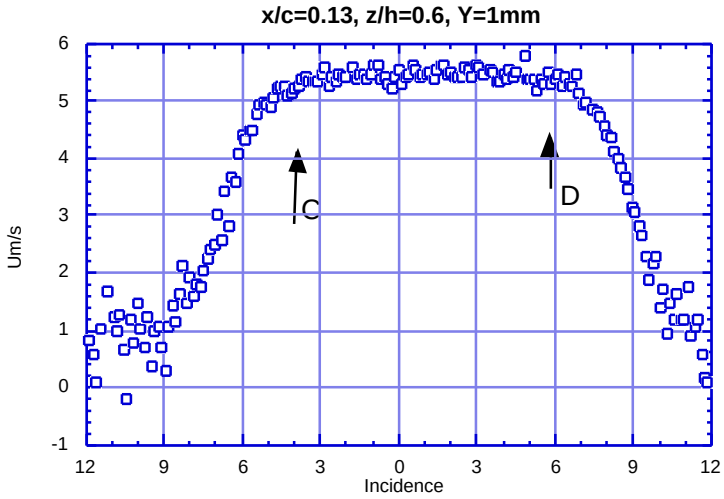
x/c=0.13, z/h=0.6, Y=1mm
Um/s
Incidence
C
D

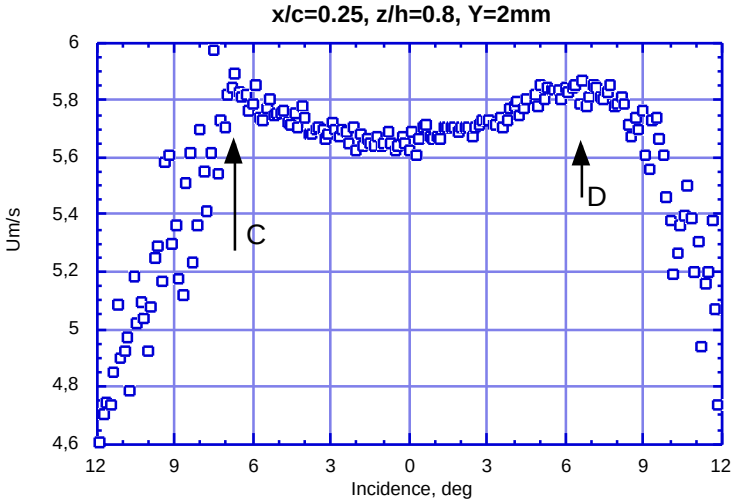
x/c=0.25, z/h=0.8, Y=2mm
Um/s
Incidence, deg
C
D

Bubble height during the oscillation at z/h=0.6

Fig26

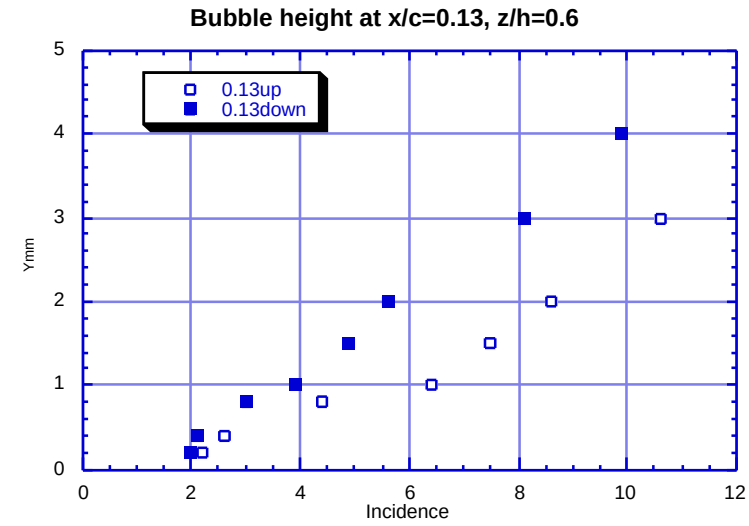

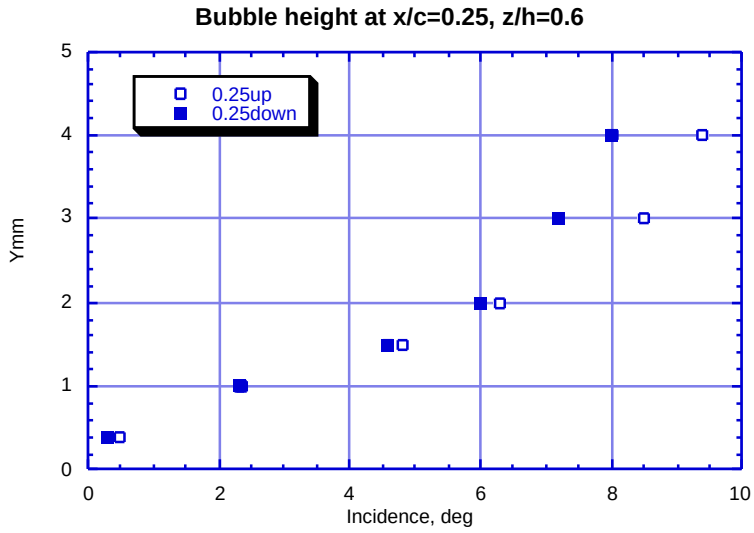

Bubble height during the oscillation at z/h=0.8

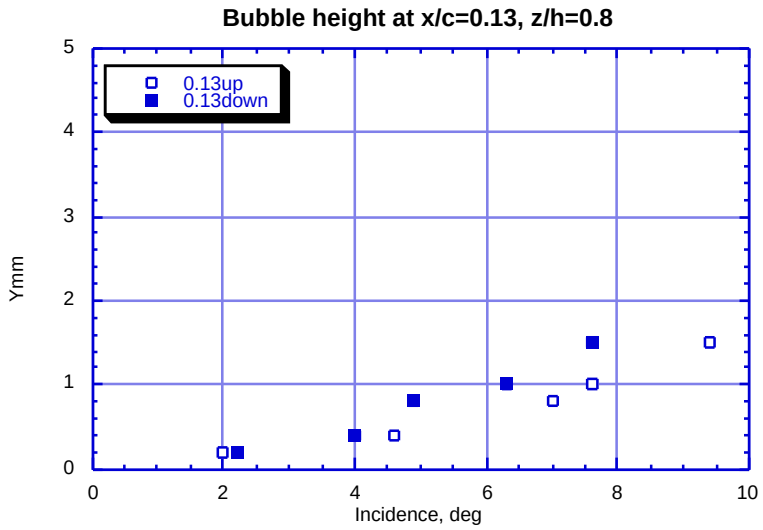

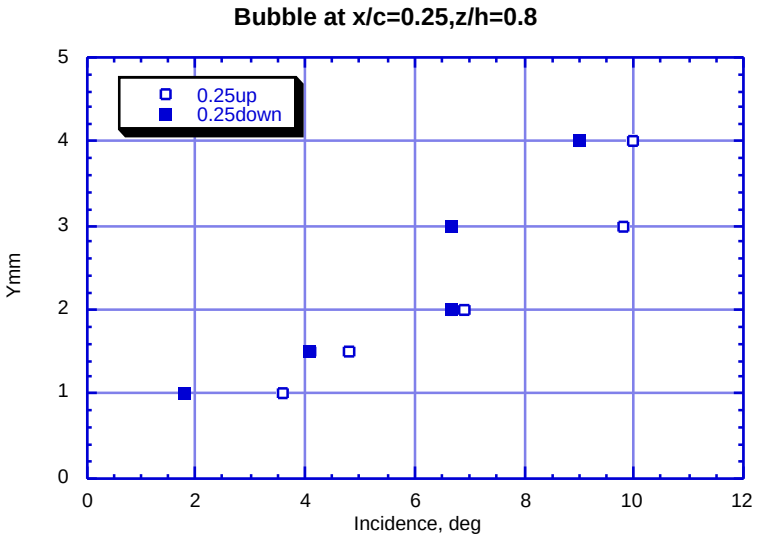

Bubble height during the oscillation

z/h=0.6

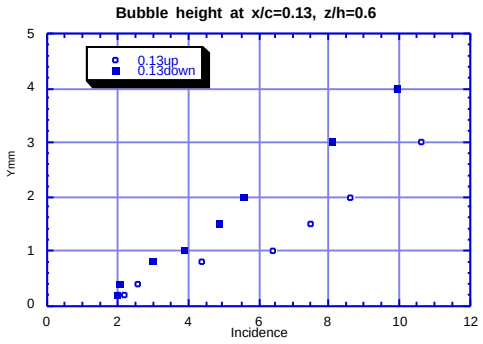

z/h=0.8

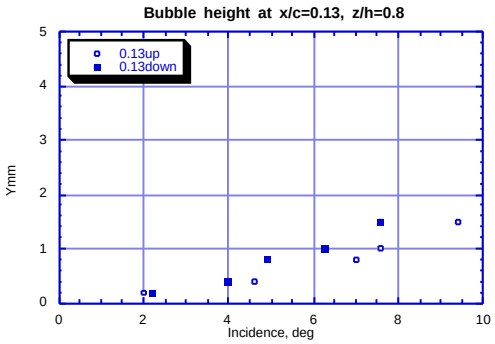

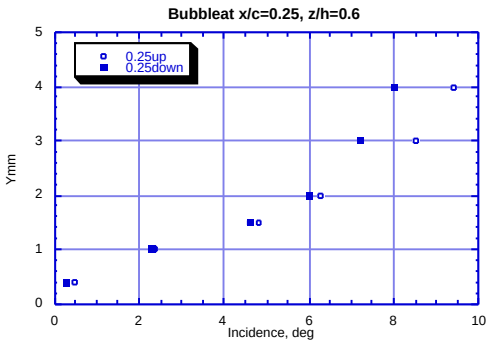

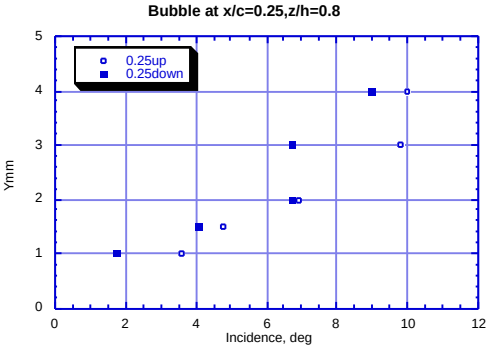

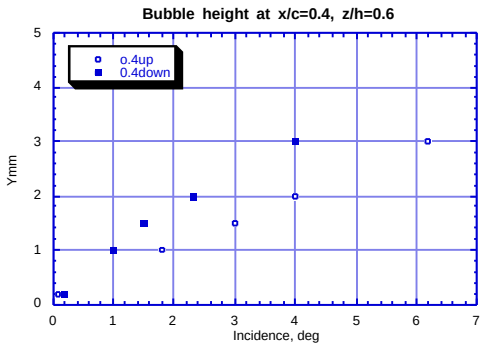

Fig. 29

Wing-tip vortex at different incidences in steady and pitching configurations

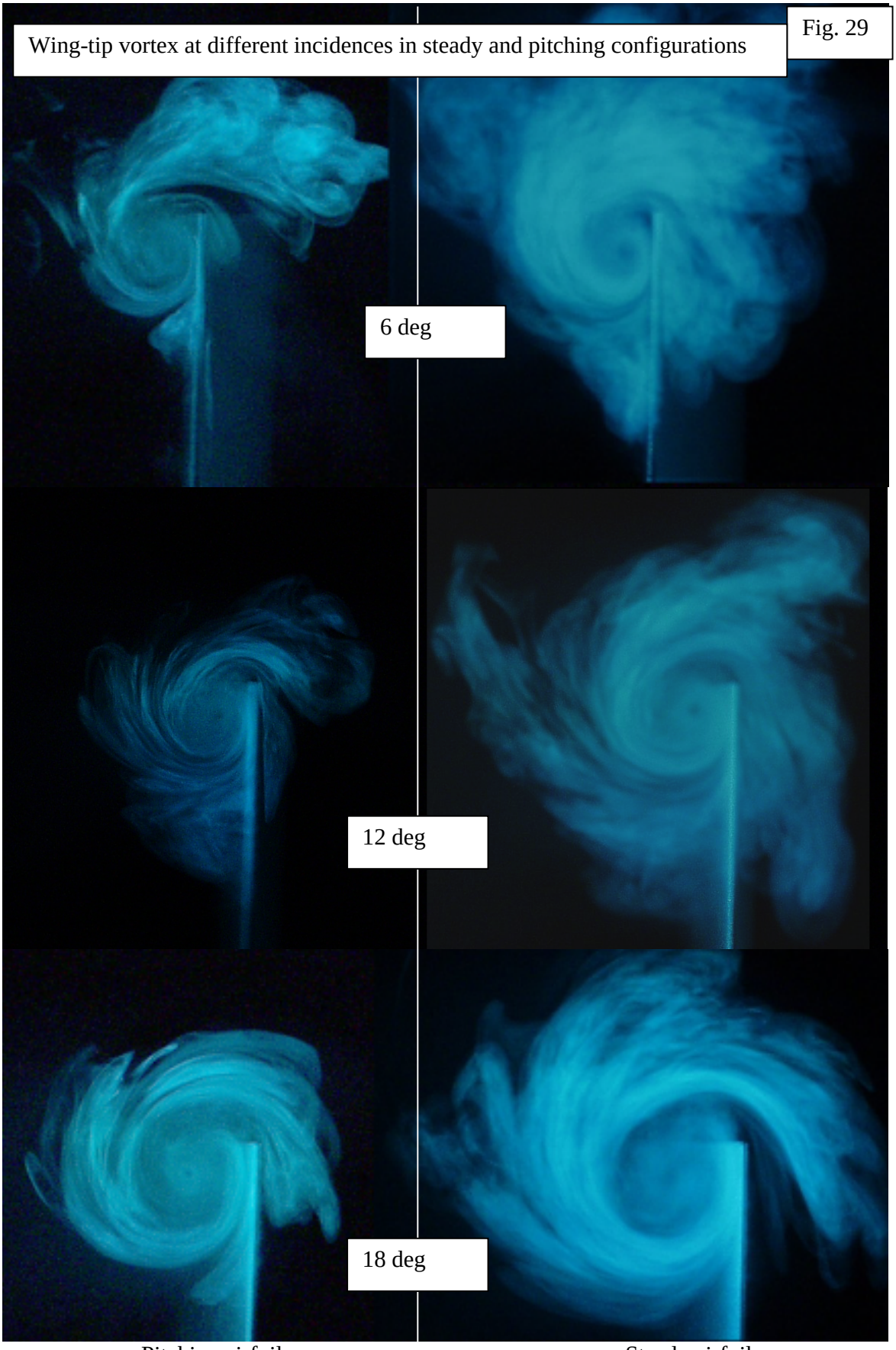

Pitching airfoil Steady airfoil

Fig. 30

Visualizations of the upper side of the pitching wing at two z/h - α=12±6

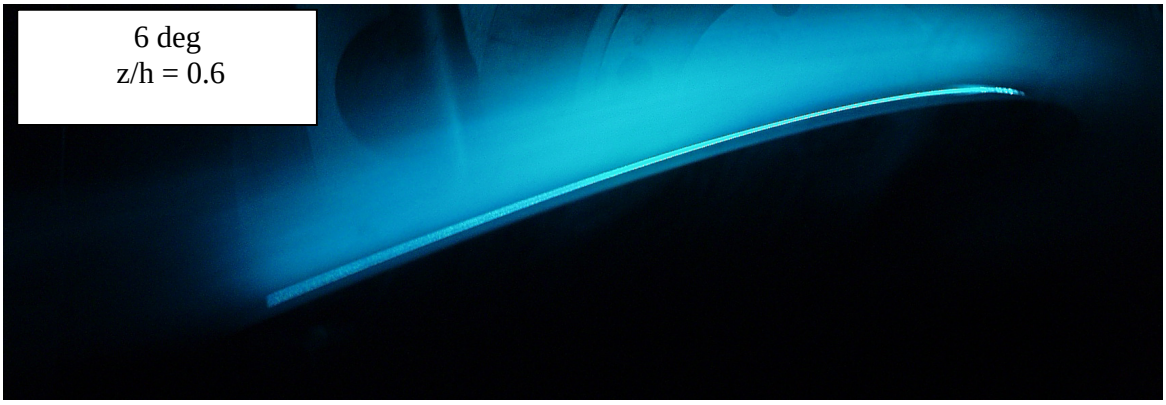

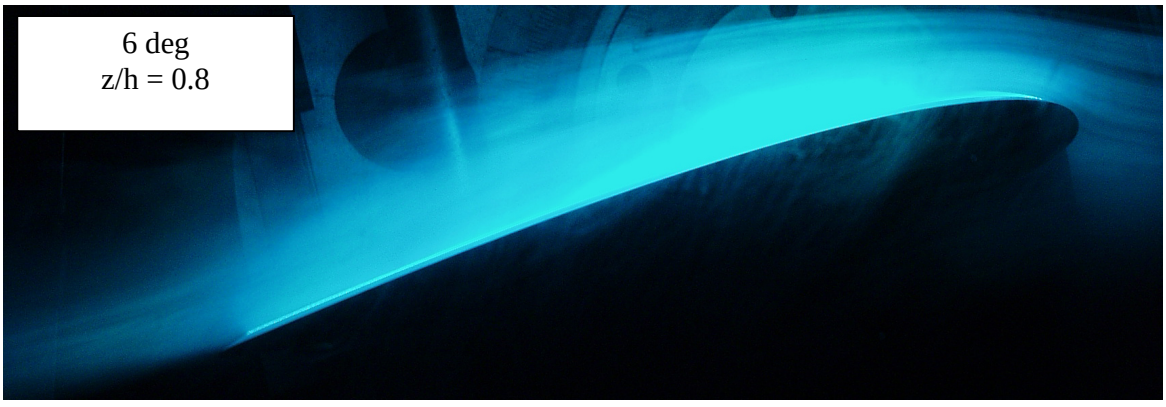

Fig. 31

Visualizations of the upper side of the pitching wing at two z/h - α=18±6

Z/h = 0.6

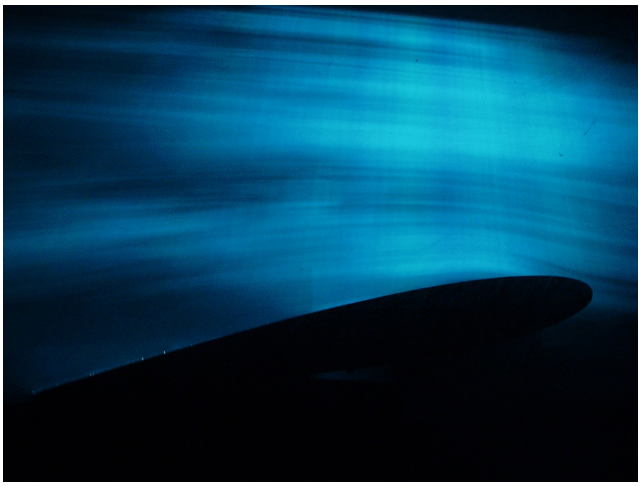

12 deg

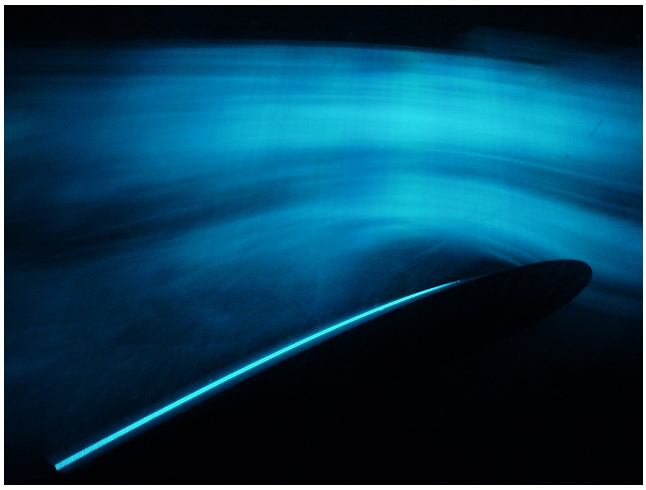

20 deg

Z/h = 0.8

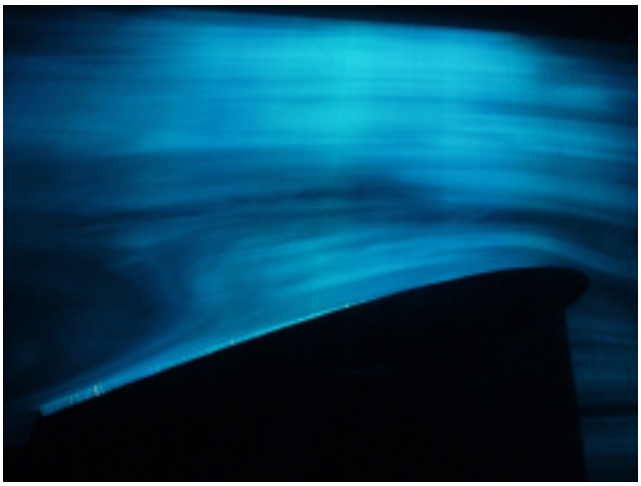

12 deg

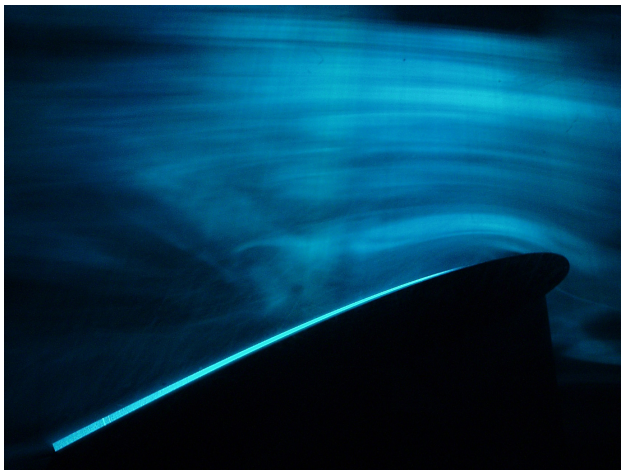

20 deg